

The catastrophic effect of mergers on the angular momentum and morphology of galaxies in EAGLE

Claudia del P. Lagos^{1,2*}, Adam R. H. Stevens³, Richard G. Bower⁴, Timothy A. Davis⁵, Sergio Contreras⁶, Nelson D. Padilla^{6,7}, Danail Obreschkow^{1,2}, Darren Croton³, James W. Trayford⁴, Charlotte Welker^{1,2}, Tom Theuns⁴

¹International Centre for Radio Astronomy Research (ICRAR), M468, University of Western Australia, 35 Stirling Hwy, Crawley, WA 6009, Australia.

²Australian Research Council Centre of Excellence for All-sky Astrophysics (CAASTRO), 44 Rosehill Street Redfern, NSW 2016, Australia.

³Centre for Astrophysics & Supercomputing, Swinburne University of Technology, Hawthorn, VIC 3122, Australia.

⁴Institute for Computational Cosmology, Department of Physics, University of Durham, South Road, Durham, DH1 3LE, UK.

⁵Astronomy, Cardiff University, Queens Buildings, The Parade, Cardiff CF24 3AA, United Kingdom.

⁶Instituto de Astrofísica, Pontificia Universidad Católica de Chile, Avda. Vicuña Mackenna 4860, 782-0436 Macul, Santiago, Chile.

⁷Centro de Astro-Ingeniería, Pontificia Universidad Católica de Chile, Avda. Vicuña Mackenna 4860, 782-0436 Macul, Santiago, Chile.

18 January 2017

ABSTRACT

We use EAGLE to explore the effect galaxy mergers have on the stellar specific angular momentum of galaxies, j_{stars} . We characterise mergers into: dry (gas-poor)/wet (gas-rich), major/minor, and by different spin alignments and orbital parameters. Our wet (dry) mergers have an average neutral gas fraction (i.e. the ratio between the neutral gas and the stellar masses of the merging system) of 1.1 (0.02), while minor (major) mergers are those with stellar mass ratios between the secondary and primary galaxy in the range 0.1 – 0.3 (≥ 0.3). We correlate the positions of galaxies in the j_{stars} -stellar mass plane at $z = 0$ with their merger history, and find that galaxies of low spins suffered dry mergers, while galaxies of normal/high spins suffered predominantly wet mergers, if any at all. The radial j_{stars} profiles of galaxies that went through dry mergers are deficient by ≈ 0.3 dex at $r \lesssim 10 r_{50}$ compared to galaxies that went through wet mergers. By studying galaxies before and after mergers, we find that dry mergers reduce j_{stars} by $\approx 30\%$, while wet mergers increase it by $\approx 10\%$, on average. The latter is connected to the build-up of the central stellar over-density by newly formed stars of high rotational speed. Moving from minor to major mergers mostly accentuates the effects above. When the spin vectors of the galaxies prior to the dry merger are misaligned, j_{stars} decreases to a greater magnitude, while in wet mergers, co-rotation and high orbital angular momentum lead to the largest j_{stars} increase. We make predictions for what would be the observational signatures in the mean j_{stars} profiles driven by dry mergers: (i) shallow radial profiles and (ii) profiles that continue to rise beyond $\approx 10 r_{50}$, both of which are significantly different from spiral galaxies.

Key words: galaxies: formation - galaxies: evolution - galaxies: fundamental parameters - galaxies: structure

1 INTRODUCTION

Galaxy mergers are a natural consequence of the hierarchical growth of structures (White & Rees 1978) and since early on have been posed to be a key physical process in their morphological transformation (e.g. Toomre & Toomre 1972; Toomre 1977; White 1978; Farouki & Shapiro 1982; Barnes 1988). Since then, galaxy mergers have become an essential process in cosmological galaxy formation models (e.g. Cole et al. 2000; Springel et al. 2001; De Lucia et al. 2006; Bower et al. 2006; Lagos et al. 2008; see Baugh 2006 for a review).

In the context of the angular momentum (AM) of galaxies,

Fall (1983) presented the first observational compilation of the specific AM of the stellar component of galaxies, j_{stars} , and its relation with stellar mass, M_{stars} . Fall (1983) found that elliptical and spiral galaxies follow parallel sequences, with the former having j_{stars} a factor of ≈ 6 lower than the latter. Fall (1983) concluded that in hierarchical cosmologies the j_{stars} values of spirals and ellipticals could be understood if spirals roughly conserve j in their formation process (see also Mo et al. 1998), while ellipticals need efficient j dissipation. Galaxy mergers are a natural dissipative phenomenon which could account for the galaxy population of low spins. Early simulations (e.g. Barnes & Efstathiou 1987; Navarro & White 1994; Heyl et al. 1996; Zavala et al. 2008) showed that dynamical friction can efficiently move high j material to the outer regions of galaxies, effectively lowering the

* E-mail: claudia.lagos@icrar.org

j_{stars} of the stellar component that is easily measurable. Later on, Romanowsky & Fall (2012), via idealised models within the Λ cold dark matter (Λ CDM) paradigm, showed that galaxy mergers can naturally explain the positions of elliptical galaxies in the $j_{\text{stars}} - M_{\text{stars}}$ plane, and that disks and bulges follow fundamentally different $j_{\text{stars}} - M_{\text{stars}}$ relations (see also Obreschkow & Glazebrook 2014). Recently, Lagos et al. (2017) found using the EAGLE hydrodynamical simulations that galaxies can have low j_{stars} and lie in the sequence of elliptical galaxies without having had any mergers. This can happen if galaxies suffer quenching before their halos reach their maximum expansion (i.e. ‘turnover’ epoch; Catelan & Theuns 1996), and thus retain a relic specific AM their halo and gas had very early on. However, Lagos et al. (2017) also showed that this only happens to $\approx 2\%$ of the galaxies, and that the preferred scenario for having a low j_{stars} continued to be galaxy mergers. In the latter, Lagos et al. (2017) showed that galaxies still need to be quenched by feedback, otherwise the continuing gas accretion and star formation dominates over the negative effect of mergers, and galaxies end up with high spins at $z = 0$.

Recent observational measurements of j_{stars} coming from integral field units (IFU) galaxy surveys, such as the Sydney-AAO Multi-object Integral field spectrograph (SAMI; Croom et al. 2012) by Cortese et al. (2016), have suggested that galaxies form a continuous sequence in the $j_{\text{stars}} - M_{\text{stars}}$ plane, instead of the two sequences originally found by Fall (1983), and thus that there may not be a fundamental distinction between bulges and disks. Cortese et al. (2016) found that the positions of galaxies in the $j_{\text{stars}} - M_{\text{stars}}$ plane were strongly correlated with the Hubble morphological type, Sèrsic index and the spin parameter of the stars λ_R , which provides a measurement of how rotationally supported a galaxy is (Emsellem et al. 2007). Cortese et al. (2016) concluded that the large-scale morphology of galaxies is regulated by their mass and dynamical state. This may not, however, be the full story. Emsellem et al. (2011) showed that early-type galaxies, from the *ATLAS*^{3D} survey, have a large variety of λ_R values and thus they cannot be seen as one uniform type of galaxy. Emsellem et al. (2011) found two broad classifications for early-type galaxies: fast and slow rotators. Some important trends found by Emsellem et al. (2011) and extended recently to higher stellar masses by Veale et al. (2017), is that the fraction of slow rotators increases steeply with stellar mass, and that the vast majority of S0 galaxies are fast rotators. All these observations measure kinematics of galaxies within a relatively small area of the galaxy (typically within 1 effective radius), which leaves open the question of whether galaxies with low spins are the result of a major loss of total j_{stars} or simply a rearrangement of j_{stars} in spite of total j conservation. These formation scenarios are not mutually exclusive, and thus one has to ask what gives rise to such variety of observed dynamical states in galaxies, and particularly, early-types.

Jesseit et al. (2009), Bois et al. (2011) and Naab et al. (2014) found that the formation paths of slow and fast rotators can be very varied. For example, Naab et al. (2014) showed that slow rotators could be formed as a result of wet major mergers, dry major mergers and dry minor mergers. In the case of wet mergers, the remnant can be either fast or slow rotators, or even disks (e.g. Bekki 1998; Springel 2000; Cox et al. 2006; Robertson et al. 2006; Johansson et al. 2009; Peirani et al. 2010; Lotz et al. 2010; Naab et al. 2014; Moreno et al. 2015; Sparre & Springel 2016b). Di Matteo et al. (2009) showed that even dry major mergers of pressure supported galaxies can result in a rotation-supported disk if the orbital AM is large enough and efficiently transferred into the orbits of stars. Many of these mergers may result in a dra-

matic change in the morphology and spin of galaxies, but ultimately mergers are one of many physical processes at play, and continuing gas accretion and star formation can reshape that remnant morphology and kinematics. Recently, Sparre & Springel (2016a) found, using cosmological hydrodynamical simulations that galaxy remnants of major mergers evolve into star-forming disk galaxies unless sufficiently strong feedback is present to prevent the disk regrowth. This feedback is an essential mechanism in the new generation of cosmological hydrodynamical simulations, such as EAGLE (Schaye et al. 2015), Illustris (Vogelsberger et al. 2014) and Horizon-AGN (Dubois et al. 2016), and most likely plays a major role in reproducing the morphological diversity seen in galaxies.

Although there is extensive literature for how different merger configurations can affect galaxies (see above), cosmological hydrodynamical simulations are necessary to realistically represent the frequency of them in a galaxy population, and thus it is the best way of shedding light on why galaxies display the diversity of j_{stars} seen in observations, especially as modern simulations reproduce the observations well (Zavala et al. 2016; Teklu et al. 2015; Pedrosa & Tissera 2015; Genel et al. 2015; Lagos et al. 2017; Sokolowska et al. 2016). This is the motivation of our work. We use the EAGLE (Schaye et al. 2015) cosmological hydrodynamical simulations to statistically study how galaxy mergers drive the positions of galaxies in the $j_{\text{stars}} - M_{\text{stars}}$ plane. We also study the main parameters determining how much spin-up or down occurs, and the cumulative effect mergers may have in the $z = 0$ galaxy population. EAGLE has a good compromise between volume, $(100 \text{ Mpc})^3$, and resolution, 700 pc, that allows to us have a statistically significant sample of galaxies (several thousands with $M_{\text{star}} > 10^9 M_{\odot}$) and with enough structural detail to be able to study mean radial j_{stars} profiles. The latter is defined as $j(r) = |J(< r)|/M(< r)$, where $J(< r)$ and $M(< r)$ are the angular momentum vector and mass enclosed in r . EAGLE has now been extensively tested against local and high-redshift observations of galaxy sizes (Furlong et al. 2015a), colours (Trayford et al. 2015), stellar masses and star formation rates (SFRs; Schaye et al. 2015; Furlong et al. 2015b), and the gas contents of galaxies (Bahé et al. 2016; Lagos et al. 2015, 2016; Crain et al. 2016), among other properties, with high success. The galaxy population in EAGLE therefore looks realistic and thus it gives us some confidence that we can use it to learn about the role of galaxy mergers in the $j_{\text{stars}} - M_{\text{stars}}$ plane. The advent of IFU surveys, such as SAMI, MaNGA (Bundy et al. 2015) and MUSE (Bacon et al. 2010), and the first global measurements of j_{stars} at high redshift (Burkert et al. 2016; Swinbank et al. submitted), make our study very timely.

This paper is organised as follows. § 2 briefly describes the details of the EAGLE simulation and introduces the parameters of mergers we will be studying. Here we also present a comparison with observational measurements of merger rates, to show that the frequency of mergers is well represented in EAGLE. In § 3 we study the cumulative effect of galaxy mergers as seen by dissecting the $z = 0$ galaxy population. We also compare the mean radial j_{stars} profiles in EAGLE with observations of early-type galaxies. We then focus on the effect galaxy mergers have on the net value of j_{stars} as well as its radial distribution in galaxies, splitting mergers into minor/major, wet/dry and in spin and orbital parameters. Here we also connect the change in j_{stars} with changes in the stellar mass distribution, and analyse the distribution of the stellar components of the galaxies prior to the merger and in the remnant. We present a discussion of our results and our main conclusions in § 4. Finally, in Appendix A we analyse the robustness of our result against the

Table 1. Features of the Ref-L100N1504 EAGLE simulation used in this paper. The row list: (1) comoving box size, (2) number of particles, (3) initial particle masses of gas and (4) dark matter, (5) comoving gravitational softening length, and (6) maximum physical comoving Plummer-equivalent gravitational softening length. Units are indicated in each row. EAGLE adopts (5) as the softening length at $z \geq 2.8$, and (6) at $z < 2.8$.

	Property	Units	Value
(1)	L	[cMpc]	100
(2)	# particles		2×1504^3
(3)	gas particle mass	[M_\odot]	1.81×10^6
(4)	DM particle mass	[M_\odot]	9.7×10^6
(5)	Softening length	[ckpc]	2.66
(6)	max. gravitational softening	[pkpc]	0.7

time resolution of the main simulation used here, while Appendix B presents additional plots that aid the interpretation of our results.

2 THE EAGLE SIMULATION

The EAGLE simulation suite¹ (described in detail by Schaye et al. 2015, hereafter S15, and Crain et al. 2015, hereafter C15) consists of a large number of cosmological hydrodynamic simulations with different resolutions, cosmological volumes and subgrid models, adopting the Planck Collaboration (2014) cosmological parameters. S15 introduced a reference model, within which the parameters of the sub-grid models governing energy feedback from stars and accreting black holes (BHs) were calibrated to ensure a good match to the $z = 0.1$ galaxy stellar mass function and the sizes of present-day disk galaxies.

In Table 1 we summarise the parameters of the simulation used in this work, including the number of particles, volume, particle masses, and spatial resolution. Throughout the text we use pkpc to denote proper kiloparsecs and cMpc to denote comoving megaparsecs. A major aspect of the EAGLE project is the use of state-of-the-art sub-grid models that capture unresolved physics. The sub-grid physics modules adopted by EAGLE are: (i) radiative cooling and photoheating, (ii) star formation, (iii) stellar evolution and enrichment, (iv) stellar feedback, and (v) black hole growth and active galactic nucleus (AGN) feedback (see S15 for details on how these are modelled and implemented in EAGLE). In addition, the fraction of atomic and molecular gas in each gas particle is calculated in post-processing following Lagos et al. (2015).

The EAGLE simulations were performed using an extensively modified version of the parallel N -body smoothed particle hydrodynamics (SPH) code GADGET-3 (Springel et al. 2008; Springel 2005). Among those modifications are updates to the SPH technique, which are collectively referred to as ‘Anarchy’ (see Schaller et al. 2015 for an analysis of the impact of these changes on the properties of simulated galaxies compared to standard SPH). We use SUBFIND (Springel et al. 2001; Dolag et al. 2009) to identify self-bound overdensities of particles within halos (i.e. substructures). These substructures are the galaxies in EAGLE.

¹ See <http://eagle.strw.leidenuniv.nl> and <http://www.eaglesim.org/> for images, movies and data products. A database with many of the galaxy properties in EAGLE is publicly available and described in McAlpine et al. (2015).

2.1 Merger parameters studied

We identify mergers using the merger trees available in the EAGLE database (McAlpine et al. 2015). These merger trees were created using the D – Trees algorithm of Jiang et al. (2014). Qu et al. (2017) describe how this algorithm was adapted to work with EAGLE outputs. Galaxies that went through mergers have more than one progenitor, and for our purpose, we track the most massive progenitors of merged galaxies, and compare the properties of those with that of the merger remnant to analyse the effect on j_{stars} . The trees stored in the public database of EAGLE connect 29 epochs. The time span between snapshots can range from ≈ 0.3 Gyr to ≈ 1 Gyr. We use these snapshots to analyse the evolution of j_{stars} in galaxies under the effect of mergers. We consider the interval between outputs appropriate, as our purpose is to analyse galaxies before and after, rather than during the merger. In order to estimate the robustness to the time interval between outputs used in the simulations for our results, in Appendix A we analyse mergers using a much finer time intervals (i.e. snippets; S15) and find that our calculations are robust and do not sensitively depend on how fine the time interval between outputs are.

We split mergers into major and minor mergers. The former are those with a stellar mass ratio between the secondary and the primary galaxy ≥ 0.3 , while minor mergers have a mass ratio between 0.1 and 0.3. Lower mass ratios are considered to be unresolved and thus are classified to be simply accretion (Crain et al. 2016).

In addition to defining minor and major mergers, we estimate the gas fraction of the merger with the aim of then classifying them as gas-rich (wet) or gas-poor (dry) mergers. This fraction is defined as:

$$f_{\text{gas,merger}} \equiv \frac{M_{\text{neutral}}^s + M_{\text{neutral}}^p}{M_{\text{stars}}^s + M_{\text{stars}}^p}, \quad (1)$$

where M_{neutral}^s and M_{neutral}^p are the neutral gas masses of the secondary and primary galaxies, respectively, while M_{stars}^s and M_{stars}^p are the corresponding stellar masses. Both set of masses are measured within an aperture of 30 pkpc. Neutral gas masses in EAGLE are calculated as in Lagos et al. (2015). In short, we use the fitting function of Rahmati et al. (2013), who studied the neutral gas fraction in cosmological hydrodynamical simulations by coupling them to a full radiative transfer calculation using TRAPHIC (Pawlik & Schaye 2008). This fitting function considers collisional ionisation, photo-ionisation by a homogeneous ultraviolet (UV) background and by recombination radiation. We adopt the model of Haardt & Madau (2001) to describe the UV background. Here, neutral gas refers to atomic plus molecular gas.

Fig. 1 shows the distribution of $f_{\text{gas,merger}}$ in three redshift bins in EAGLE. We find that the distributions are mostly bimodal, and we use this fact to define gas-rich ($f_{\text{gas,merger}} \geq 0.5$) and gas-poor ($f_{\text{gas,merger}} \leq 0.2$) mergers, as shown by the vertical dotted lines. From now on, we name these two sub-samples as wet and dry mergers, respectively. At $0 \leq z \leq 3$, these two samples are made of 2,677 and 1,775 mergers, respectively, and have median $f_{\text{gas,merger}}$ of 1.1 and 0.02, respectively. In the literature, ‘dry’ mergers usually refer to galaxies completely devoid of gas (e.g. Makino & Hut 1997; Naab et al. 2006a; Taranu et al. 2013). However, the reason behind that definition was mostly technical: mergers were studied with collisionless simulations. However, in reality galaxies are expected to have some gas, even in the regime of ‘red and dead’ passive galaxies, as shown by the observations of ATLAS^{3D} (Young et al. 2011; Serra et al. 2012). EAGLE allows

us to define ‘dry’ mergers in a more realistic fashion, by simply imposing them to be gas poor. When we dissect $f_{\text{gas,merger}}$ into the contributions from the primary (the one with the highest stellar mass) and secondary galaxies, we find that at any redshift the total gas fraction is dominated by the primary galaxy. In EAGLE we find a good correlation between the gas fractions of the primary and the secondary galaxy, which is stronger at high redshift. This correlation is a consequence of the ‘conformity’ of the galaxy population (i.e. gas-rich galaxies tend to be surrounded by gas-rich galaxies; Kauffmann et al. 2013; Wang et al. 2015; Hearin et al. 2016).

Throughout this paper we study j of the stars in three apertures, using all the star particles within the half-mass radius of the stars, $j_{\text{stars}}(r_{50})$ (close to what most observers have; e.g. Emsellem et al. 2011; Cortese et al. 2016; Veale et al. 2017), within 5 times r_{50} , $j_{\text{stars}}(5r_{50})$, and using all of the star particles in the subhalo, $j_{\text{stars}}(\text{tot})$, as well as the full radial profiles. We calculate radial j profiles as in Lagos et al. (2017), which effectively means that we are measuring a mass-weighted average j_{stars} within r (i.e. $\equiv |J(< r)|/M(< r)$). We will refer to these measurements as ‘mean radial j_{stars} profiles’. Lagos et al. (2017) showed that $j_{\text{stars}}(r_{50})$ converges in EAGLE at $M_{\text{stars}} \gtrsim 10^{9.5} M_{\odot}$, and thus we limit our sample only to galaxies with stellar masses above that threshold. We calculate two angles that determine how mergers are oriented: the first, θ_{spin} , is the angle subtended between the $\vec{j}_{\text{stars}}(\text{tot})$ vectors of the two galaxies that are about to merge, and the second, θ_{orb} , is the angle between $\vec{j}_{\text{stars}}(\text{tot})$ of the primary galaxy and the orbital AM vector,

$$\theta_{\text{spin}} = \arccos \left[\hat{j}_{\text{stars}}^s(\text{tot}) \cdot \hat{j}_{\text{stars}}^p(\text{tot}) \right], \quad (2)$$

and

$$\theta_{\text{orb}} = \arccos \left[\hat{j}_{\text{orbital}} \cdot \hat{j}_{\text{stars}}^p(\text{tot}) \right], \quad (3)$$

where $\vec{j}_{\text{stars}}^s(\text{tot})$ and $\vec{j}_{\text{stars}}^p(\text{tot})$ are the normalised j_{stars} vectors of the secondary and primary galaxies, respectively, and $\vec{j}_{\text{orbital}} = \vec{r} \times \vec{v}$. Here, \vec{r} and \vec{v} are the position and velocity vectors of the secondary galaxy in the rest-frame of the primary one, calculated in the last snapshot the two galaxies were identified as separate objects. Galaxy growth produced by gas accretion and star formation will be termed ‘smooth accretion’ during the rest of the paper.

The top and middle panels of Fig. 2 show the merger rate density of minor and major mergers in (primary) galaxies with $M_{\text{stars}} > 10^{9.5} M_{\odot}$ as a function of redshift, respectively, and split into wet and dry mergers. The frequency of minor and major mergers are relatively noisy due to the small volume of the simulation and the relatively high stellar mass threshold we are applying to our galaxy sample. The frequency of dry mergers increases from $z = 2.5$ down to $z = 1$ in both minor and major mergers, with a approximately constant frequency at $z < 1$, while the frequency of wet mergers decreases steadily towards $z = 0$. The latter is driven by the EAGLE galaxies having neutral gas fractions that decrease with time (Lagos et al. 2015, 2016). In the bottom panels of Fig. 2 we show the frequency of mergers split by their spin orientation and orbital alignment, respectively. In the case of spin alignments, we define co-rotating, perpendicular and counter-rotating mergers as those with $\cos(\theta_{\text{spin}}) > 0.7$ (angles between $0 - 45$ degrees), $-0.15 < \cos(\theta_{\text{spin}}) < 0.15$ (angles between $81 - 99$ degrees) and $\cos(\theta_{\text{spin}}) < -0.7$ (angles between $135 - 180$ degrees), respectively. Randomly oriented mergers in three dimensions would imply a uniform distribution in $\cos(\theta_{\text{spin}})$; hence the number of mergers in these equal ranges (0.3 in $\cos(\theta_{\text{spin}})$) directly show their relative frequency. We find in

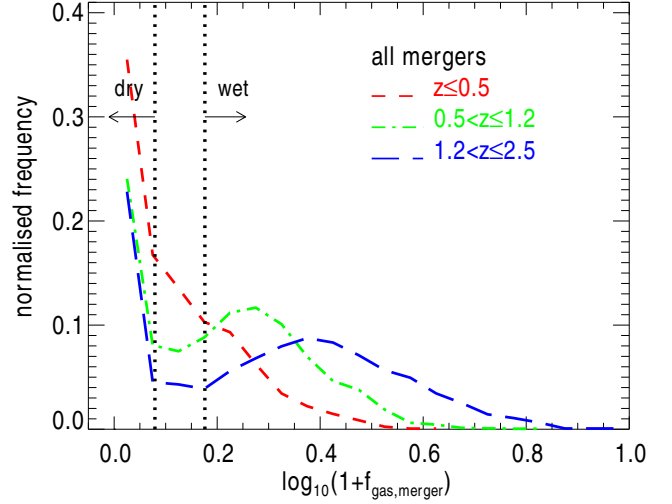


Figure 1. Gas fraction distribution of mergers in EAGLE in 3 redshift bins, as labelled. Distributions are mostly bimodal, and we use this to define gas-rich (wet) and gas-poor (dry) mergers in EAGLE (shown as dotted lines).

EAGLE that perpendicular mergers are ≈ 1.3 times more common than co-rotating mergers, but counter-rotating mergers are ≈ 3.4 and ≈ 2.6 times less common than perpendicular and co-rotating mergers, respectively. In the case of orbital alignments, we define co-planar mergers as those with $|\cos(\theta_{\text{orb}})| \geq 0.7$, while perpendicular mergers have $|\cos(\theta_{\text{orb}})| \leq 0.3$. Here we find that co-planar mergers are ≈ 1.5 more frequent than perpendicular ones. The trends we see here for θ_{spin} and θ_{orb} are consistent with the trends presented by Welker et al. (2015) using the Horizon-AGN simulation. Welker et al. (2015) showed that satellite galaxies on a decaying orbit towards the central galaxy tend to align with the galactic plane of the central in a way that, by the time they merge, are most likely to come in an orbit aligned with the galactic plane of the primary, which here would appear as a high value of $\cos(\theta_{\text{orb}})$. Welker et al. (2015) also found that mergers taking place in filaments are more likely to be of galaxies with $\cos(\theta_{\text{spin}}) \approx 0$ if the primary galaxy is a passive, spheroidal galaxy, while co-rotation is expected if the primary galaxy is a spiral, star-forming galaxy. The frequencies we report in the bottom panels of Fig. 2 are consistent with this picture.

Fig. 3 compares the major merger rate of EAGLE galaxies with $M_{\text{stars}} \geq 10^{11} M_{\odot}$ at different redshifts against a compilation of observations. Here we employ 3 different stellar mass ratios to define major mergers: $\geq 1 : 5$, $\geq 1 : 4$ and $\geq 1 : 3$, with the aim of showing the systematic variations produced by the definition of major merger (i.e. observations adopt slightly different mass ratios to define major mergers). The observations of Fig. 3 present measurements of merger rates from the characterisation of pair frequency (Bundy et al. 2009; Bluck et al. 2009; López-Sanjuan et al. 2012; Robotham et al. 2014), as well as from the identification of galaxies with disturbed morphologies (Bluck et al. 2012). Both set of measurements agree remarkably well. We find that the major merger rate of massive galaxies is in excellent agreement with the observations. For our purpose this means that the effect of galaxy mergers on the AM of galaxies is not going to be over(under)-represented, which would be the case if EAGLE was predicting a higher (lower) merger rate compared to observations.

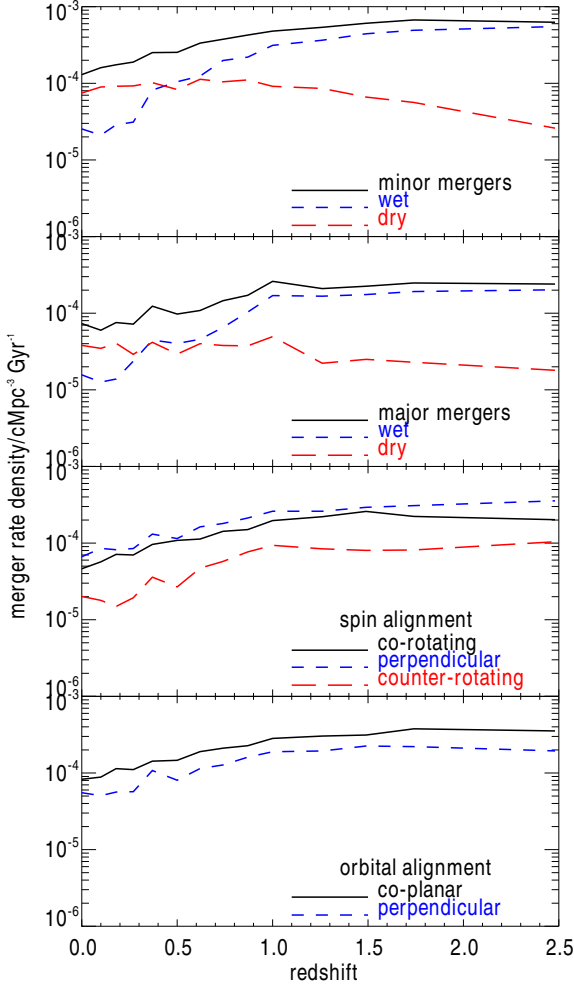


Figure 2. Merger rate density as a function of redshift in EAGLE. The top panel shows minor mergers and the subsamples of wet and dry minor mergers, as labelled. The middle panel is the same but for major mergers, while the bottom panels show mergers split into spin (i.e. co-rotating, perpendicular and counter-rotating) and orbital (i.e. co-planar and perpendicular) alignments, respectively.

3 THE EFFECT OF MERGERS ON THE STELLAR SPECIFIC AM OF GALAXIES THROUGHOUT COSMIC TIME

In this section we analyse the effect galaxy mergers of different nature have on the specific AM of galaxies. In § 3.1, we present an analysis of the accumulated effect of mergers by studying the galaxy population at $z = 0$. In § 3.2 we analyse the effect of mergers by comparing measurements of galaxy properties before and after the mergers, and how these depend on the nature of the merger. In § 3.3 we analyse the radial rearrangement of j_{stars} as a result of mergers.

3.1 The net effect of galaxy mergers seen at $z = 0$

The top-left panel of Fig. 4 shows how the galaxy merger rate changes with the position of galaxies in the $j_{\text{stars}}(r_{50})$ - M_{stars} plane. We define the average merger rate of individual galaxies as the number of mergers divided by the stellar-mass weighted age. Here we do not distinguish recent from far in the past mergers, but

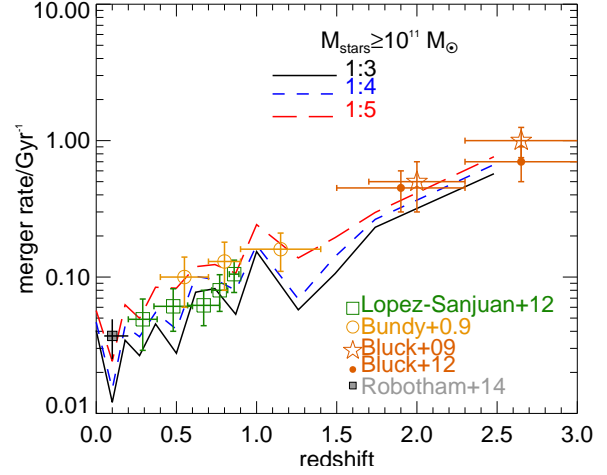


Figure 3. Merger rate in galaxies with $M_{\text{stars}} \geq 10^{11} M_{\odot}$ in EAGLE as a function of redshift. We show merger ratios $\geq 1 : 3$ (solid line), $\geq 1 : 4$ (short-dashed line) and $\geq 1 : 5$ (long-dashed line). We also show the observational measurements of Bundy et al. (2009), Bluck et al. (2009), López-Sanjuan et al. (2012), Bluck et al. (2012) and Robotham et al. (2014). Most of these observational works assume major mergers are those with stellar mass ratios $\geq 1 : 4$. EAGLE predicts major merger rates of massive galaxies that are in excellent agreement with the observations in the entire redshift range where measurements are available.

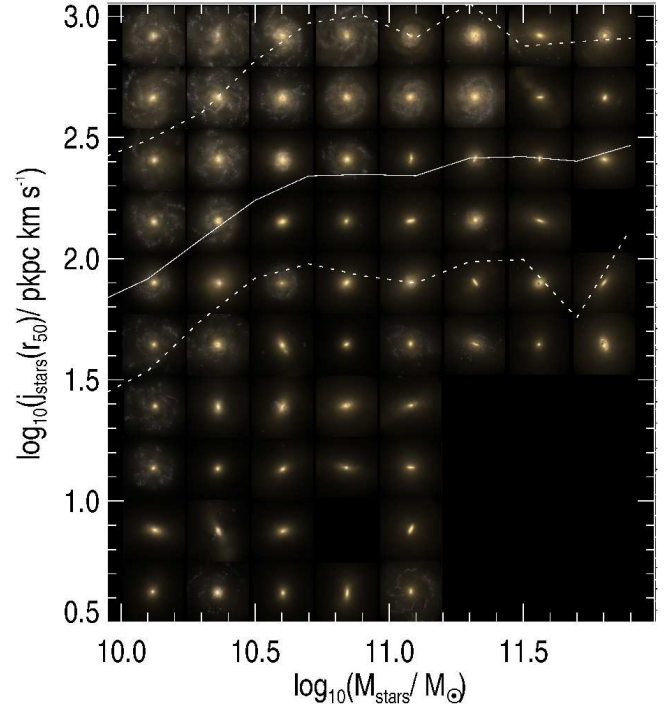


Figure 5. Visualisation of the optical morphology of galaxies in the $j_{\text{stars}}(r_{50})$ - M_{stars} plane at $z = 0$. We randomly select galaxies in 10 bins of $\log_{10}(j_{\text{stars}}(r_{50}))$ and 8 bins of $\log_{10}(M_{\text{stars}})$ in the range $10^{0.5} - 10^3 \text{ pkpc km s}^{-1}$ and $10^{10} - 10^{12} M_{\odot}$, respectively, and show here their synthetic g, r, i face-on optical images. Only bins with ≥ 3 galaxies are shown here. These images are 60 pkpc on a side and are publicly available from the EAGLE database (McAlpine et al. 2015). The solid and dotted lines show the median and the 16th to 84th percentile range.

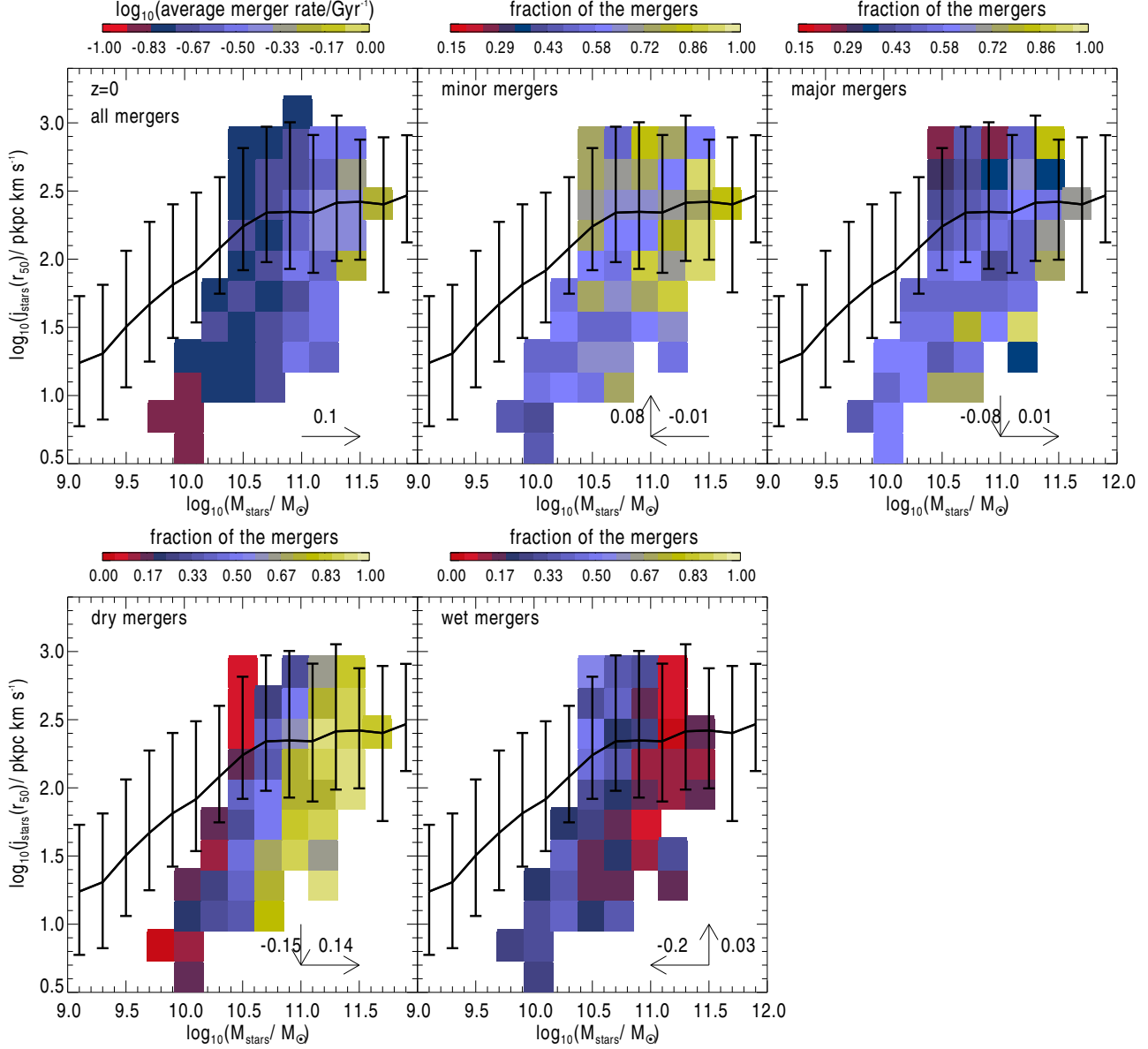


Figure 4. *Top panels:* The specific AM of the stars measured with all the particles within the half-mass radius of the stellar component as a function of stellar mass at $z = 0$ for galaxies with $M_{\text{stellar}} > 10^9 M_{\odot}$ in EAGLE. The line with errorbars in all of the panels show the median and the 16th to 84th percentile range of all galaxies at $z = 0$. In the left panel we colour bins (with ≥ 5 galaxies) in which more than 50% of the galaxies have suffered mergers, by the average merger rate per galaxy they had during their lifetimes. In the middle and right panels we colored those same bins by the fraction of the mergers that were minor and major, respectively. By construction, the fractions of the middle and right panels in each 2-dimensional bin add up to 1. *Bottom panels:* As in the top middle and right panels, but for the fraction of the mergers that were dry and wet, respectively. The arrows in each panel indicate the directions in which the frequency of the respective merger type increases and the number next to the arrows show the best fit power-law index for the relations: average merger rate $\propto M^{\alpha}$, merger fraction $\propto M^{\alpha}$ and merger fraction $\propto j^{\alpha}$.

just count their occurrence. We colour only those bins in which at least 50% of the galaxies have undergone mergers during their lifetimes. This is why below $M_{\text{stars}} \approx 10^{10} M_{\odot}$ there are very few coloured bins, i.e. most galaxies here did not undergo mergers. At $10^{10} M_{\odot} \lesssim M_{\text{stars}} \lesssim 10^{10.5} M_{\odot}$ mostly galaxies with low spins have a significant contribution from mergers. These galaxies are hosted by halos that are on average 20% more massive than those of galaxies of the same stellar mass but that never had mergers. At $M_{\text{stars}} \gtrsim 10^{10.5} M_{\odot}$ the vast majority of galaxies had at least one merger by $z = 0$. The merger rate increases with increasing mass

(best power-law fit is $\propto M_{\text{stars}}^{0.1}$), and no clear correlation is seen with $j_{\text{stars}}(r_{50})$ at fixed stellar mass.

In the top middle and right panels of Fig. 4 we calculate the fraction of the mergers shown in the left panel that were minor and major, respectively. We also performed power-law best fits to the relationship between the merger fraction and M_{stars} and $j_{\text{stars}}(r_{50})$ to quantify the trends. The best fit power-law indices are shown in each panel of Fig. 4.

The fraction of major and major mergers very weakly increase and decrease, respectively, with increasing stellar mass (see power-

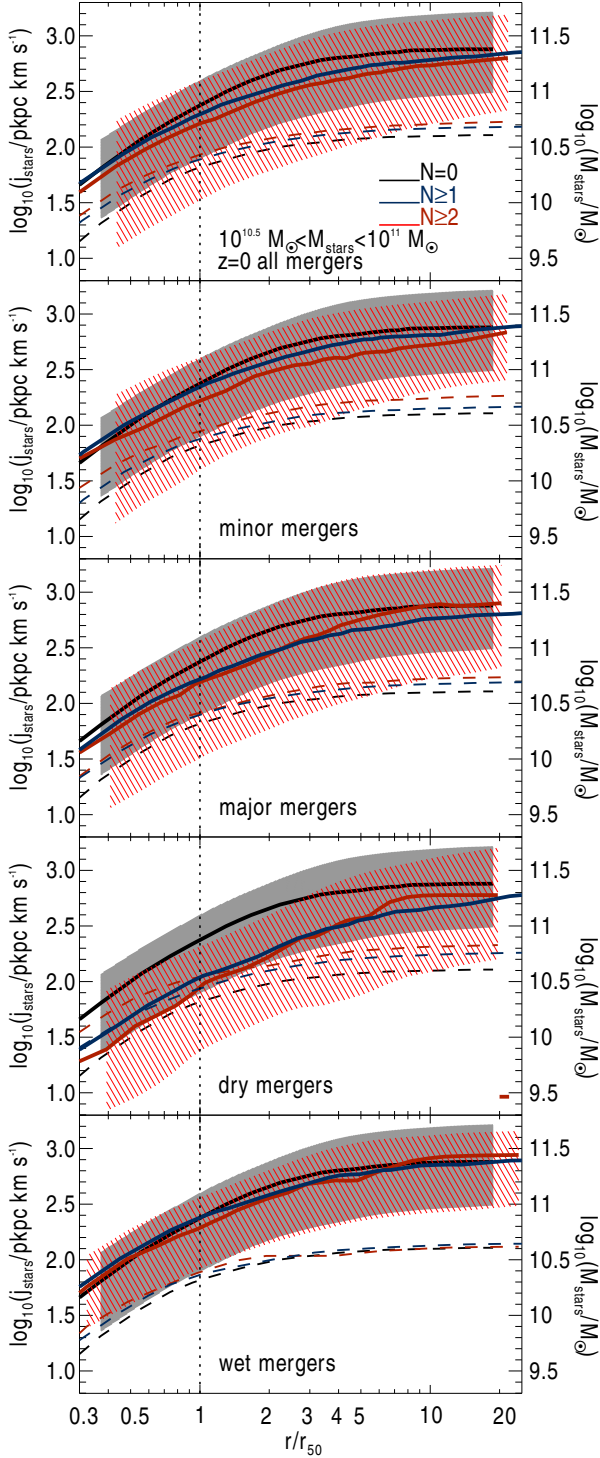


Figure 6. *Top panel:* j_{stars} (solid lines) and M_{stars} (dashed lines) measured within r as a function of r in units of r_{50} for galaxies at $z = 0$ with total stellar masses in the range $10^{10.5} M_{\odot} - 10^{11} M_{\odot}$ that have gone through different numbers of galaxy mergers, as labelled. Lines show the median of the profiles of galaxies, while the shaded regions show the 16th to 84th percentile range, plotted only for $N_{\text{mergers}} = 0, \geq 2$, for clarity. The scale of j_{stars} and M_{stars} are marked in the left and right axis, respectively. *Other panels:* As in the top panel, but distinguishing between minor, major, dry and wet mergers, as labelled. This figure shows that galaxy mergers generally lead to a deficit of j_{stars} at $r \lesssim 10 r_{50}$, with dry mergers causing pronounced deficits of ≈ 0.5 dex. At sufficiently large radii, j_{stars} converges to a value set by the dark matter halo.

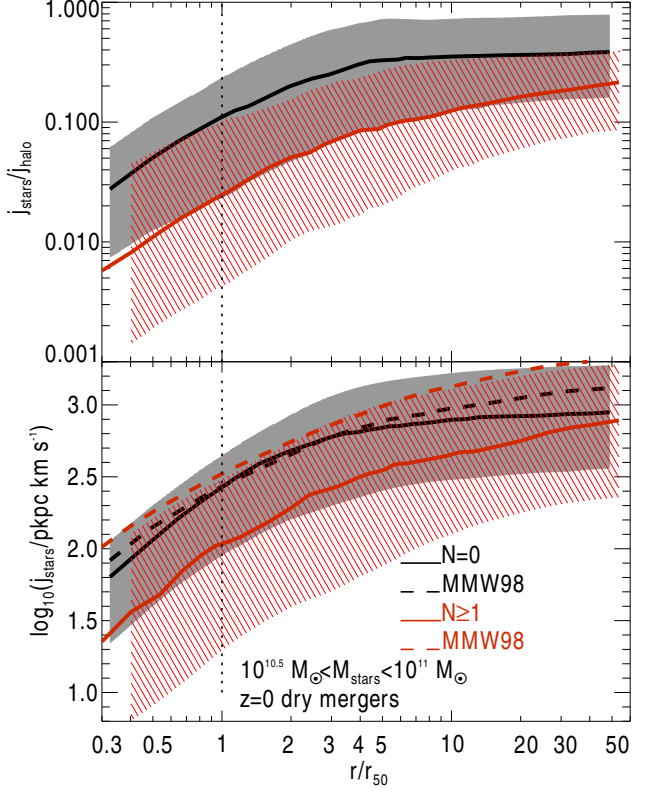


Figure 7. *Top panel:* As in Fig. 6 for the subsample of central galaxies at $z = 0$ that have not suffered a merger (black solid line) and those that went through at least one dry merger (red solid line), and that have stellar masses in the range $10^{10.5} M_{\odot} - 10^{11} M_{\odot}$. Here we show j_{stars} in units of the specific AM of the dark matter halo, j_{halo} , calculated with all dark matter particles within the virial radius. Galaxies that did not have a merger typically have j_{stars} increasing from ≈ 0.1 at r_{50} to $\approx 0.4 j_{\text{halo}}$ at $10 r_{50}$, while galaxies that had at least one dry merger go from ≈ 0.02 to $\approx 0.2 j_{\text{halo}}$ in the same radii range, on average. *Bottom panel:* As Fig. 6 but for the subsample of galaxies shown in the top panel. The dashed lines show the prediction from Mo et al. (1998) for self-gravitating disks in Navarro et al. (1997) DM halo profiles (Eq. 4). We find that the subsample of galaxies with no mergers follow the theoretical expectation closely, while the subsample of dry mergers has ≈ 0.6 dex less j_{stars} , deviating from the idealised case of specific AM conservation.

law indices in Fig. 4). We also see a slightly stronger trend with $j_{\text{stars}}(r_{50})$: at fixed stellar mass the frequency of major and minor mergers decrease and increase, respectively with increasing $j_{\text{stars}}(r_{50})$. The directions in which the frequency of mergers increase are shown as arrows in Fig. 4.

In the bottom panels of Fig. 4 we split the mergers into dry and wet, following the definition of Fig. 1. Here we see stronger trends with both M_{stars} and $j_{\text{stars}}(r_{50})$. In the case of dry mergers, we find an increase in their frequency with increasing stellar mass, and we identify a significant gradient of an increasing fraction of dry mergers with decreasing $j_{\text{stars}}(r_{50})$ at fixed stellar mass (see power-law indices in the bottom panel of Fig. 4). In the case of wet mergers, we find that their fraction increases with decreasing stellar mass and increasing $j_{\text{stars}}(r_{50})$. The latter though is a very weak trend. Fig. 4 indicates that the gas fraction involved in the merger (i.e. whether it is wet or dry) is more important than the mass ratio (i.e. whether it is a major or a minor merger) for the current $j_{\text{stars}}(r_{50})$ of galaxies. We examine the same plots for

j_{stars} measured within $5r_{50}$ and find the same trends (not shown here), and thus conclude that these trends are valid for j_{stars} inside the inner and outer regions of galaxies. These results suggest that galaxy mergers can have a devastating effect on the specific AM of galaxies, but with the exact effect strongly depending on the nature of the merger.

Lagos et al. (2017) found that the positions of galaxies in the $j_{\text{stars}}(r_{50})$ - M_{stars} plane are strongly correlated with a galaxy's gas fraction, stellar age, stellar concentration, optical colour and V/σ , all of which are usually used to distinguish early and late type galaxies. In Fig. 5 we explicitly show how the morphology of galaxies changes in this plane. To construct this figure we randomly selected galaxies in 10 bins of $\log_{10}(j_{\text{stars}}(r_{50}))$ and 8 bins of $\log_{10}(M_{\text{stars}})$ in the ranges $10^{0.5} - 10^3 \text{ pkpc km s}^{-1}$ and $10^{10} - 10^{12} M_{\odot}$, respectively, and selected their synthetic g, r, i images from the EAGLE database, described in McAlpine et al. (2015). These images are face-on views of the selected galaxies and are 60 pkpc on a side (see McAlpine et al. 2015 for a description of how these images were produced). This figure shows that at fixed M_{stars} , galaxies go from being red spheroidals at low $j_{\text{stars}}(r_{50})$ to being grand-design spirals at high $j_{\text{stars}}(r_{50})$ in the stellar mass range $10^{10} M_{\odot} \lesssim M_{\text{stars}} \lesssim 10^{11} M_{\odot}$. At higher stellar masses, galaxies with high $j_{\text{stars}}(r_{50})$ appear more like defunct spirals, with little star formation and aging disks. If we follow the median $j_{\text{stars}}(r_{50})$, one sees that galaxies go from being preferentially spiral/disk-dominated at $M_{\text{stars}} \approx 10^{10} M_{\odot}$ to spheroids at $M_{\text{stars}} \gtrsim 10^{11.5} M_{\odot}$. Given the strong correlation between the positions of galaxies in the $j_{\text{stars}}(r_{50})$ - M_{stars} plane with the frequency of wet/dry mergers, and with the morphologies of galaxies, one would expect morphologies to be connected to wet/dry mergers. Rodriguez-Gomez et al. (2016) showed that the morphologies of galaxies are connected with the merger history in the Illustris simulation, but they could only determine a clear correlation in massive galaxies, $M_{\text{star}} \geq 10^{11} M_{\odot}$, due to predominance of dry mergers and ex-situ formation of the stars. Rodriguez-Gomez et al. (2016) did not dissect galaxy mergers in many parameters, and thus they were unable to find finer correlations between mergers and morphology. Our results in EAGLE suggest that the morphology of galaxies, as well as their j_{stars} , sensitively depend on the type of the merger (dry/wet minor/major merger, and on the spin alignment and orbital parameters). We will explore this connection and the effect on $j_{\text{stars}}(r_{50})$ in § 3.2.

We now examine the mean radial j_{stars} profiles of galaxies at $z = 0$ in Fig. 6 in a narrow range of stellar mass, $10^{10.5} M_{\odot} \lesssim M_{\text{stars}} \lesssim 10^{11} M_{\odot}$. In the same Figure we also show the cumulative radial profile of M_{stars} . In the top panel we show how different the radial j_{stars} profile is in galaxies that suffered different numbers of mergers, without yet distinguishing the nature of the merger. Increasing the frequency of mergers has the effect of flattening the radial j_{stars} profile, in a way that galaxies that went through a higher number of mergers have a deficit of j_{stars} at $0.5 r_{50} \lesssim r \lesssim 10 r_{50}$ as large as ≈ 0.3 dex compared to their counterparts of the same mass but that did not go through mergers. At sufficiently large radii, j_{stars} converges so that galaxies with different number of mergers have a similar $j_{\text{stars}}(\text{tot})$. This suggests that the most important effect of mergers is in the radial structure of j_{stars} rather than the total j_{stars} . The stellar mass cumulative profile of galaxies is also shallower when the frequency of mergers increases, which means that a larger fraction of the stellar mass is locked up in the outskirts of galaxies. Although there is a small tendency for galaxies that went through more mergers to have a larger r_{50} , the trends here are not affected by this, as the differences in the radial profiles are

very similar even when we do not normalise the x -axis by r_{50} . By splitting mergers into minor and major (second and third panels of Fig. 6) we find that galaxies that had one major merger can have a deficit in j_{stars} similar to those that had two minor mergers, and increasing the frequency of major mergers does not seem to have the cumulative effect that is seen for minor mergers. EAGLE galaxies that had major mergers could have had minor mergers too, while for the sample of minor mergers, we remove all galaxies that had at least one major merger.

We then analyse mergers split into dry and wet in the bottom panels of Fig. 6 and find that *dry mergers have a catastrophic* effect on j_{stars} from the centre all the way to $\approx 20 r_{50}$. The deficit of j_{stars} compared to galaxies without a merger is as large as ≈ 0.5 dex. Also note that the stellar mass cumulative profile is much shallower for galaxies that went through a dry merger. In the case of wet mergers we see the exact opposite. Very little difference is found between galaxies that did not suffer a merger, and those that suffered one, two or more wet mergers. This reinforces the conclusion that to j_{stars} of a galaxy, what matters most is whether the merger is dry or wet. We will show in Fig. 10 that this is also true when we study j_{stars} before and after the merger. Note that in the case of dry mergers, we still see that the mean radial j_{stars} profile converges at sufficiently large radii to a $j_{\text{stars}}(\text{tot})$ that does not strongly depend on the merging history of galaxies.

3.1.1 The galaxy/halo specific AM connection

When we compare j_{stars} of the galaxies with the specific AM of their dark matter halos in the top panel of Fig. 7 we find that galaxies that went through at least one dry merger on average have a $j_{\text{stars}}(\text{tot})$ that is 5 times smaller than that of their halo, while galaxies that did not go through a merger typically retain $\approx 40 - 50\%$ of their halo j . This latter result agrees very well with the prediction by Stevens et al. (2016a) for spiral galaxies. With a semi-analytic model, those authors evolved the one-dimensional structure of discs in a series of annuli of fixed specific AM. They assumed that when gas cooled or accreted onto a galaxy that it carried the same total j of the halo *at that time* in both magnitude and direction, and that is was distributed exponentially. Stars were formed in annuli that were Toomre unstable or had sufficient H_2 . At $z = 0$, they found spiral galaxies (which had not suffered dry mergers) had $j_{\text{stars}}/j_{\text{halo}} = 0.4 \pm 0.29$, independent of galaxy mass (see their Fig. 13). Despite the completely different methodology, this aligns almost perfectly with the result of EAGLE galaxies that have not participated in a dry merger.

Fall (1983) and Romanowsky & Fall (2012) suggested that spiral galaxies needed to have a j_{stars} close to that of their halo, while ellipticals had to lose 90% of their j , postulating a fundamental difference between the two galaxy populations. The conclusions reached by these authors were biased by the available observations, that in the best case went out to $\approx 10 r_{50}$. According to EAGLE, early-type galaxies only reach ≈ 0.1 of the expected halo j at $r \approx 10 r_{50}$, on average. EAGLE galaxies show that j_{stars} continues to increase out to much larger radii due to the effect of adding halo stars. EAGLE predicts that this difference shrinks at larger radii, although still not converging to a fraction of j_{halo} as high as galaxies with no mergers in their lifetime. Early simulations of mergers predicted that dynamical friction could redistribute AM from the inner to the outer regions (e.g. Barnes & Efstathiou 1987; Navarro & White 1994; Heyl et al. 1996). From those simulations one would expect a net weak conservation of j . Our findings with EAGLE show a significant disparity between the stellar and the halo

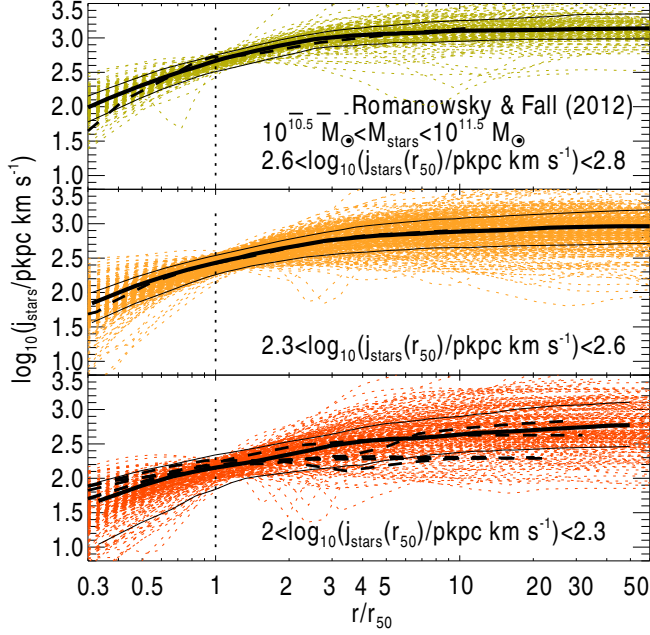


Figure 8. Mean radial j_{stars} profiles for galaxies in EAGLE at $z = 0$ and with stellar masses in the range $10^{10.5} M_{\odot} - 10^{11.5} M_{\odot}$ in 3 bins of $j_{\text{stars}}(r_{50})$, as labelled in each panel. In dotted lines we show all galaxies in that range, while the thick and thin solid lines show the median, and the 16th and 84th percentile ranges, respectively. We show observations of early-type galaxies from Romanowsky & Fall (2012) as dashed lines. Their sampled galaxies have stellar masses in the range we selected here, and we show each galaxy in their corresponding bin of $j_{\text{stars}}(r_{50})$. Here we only show the median measurement, but errorbars around those measurements can be as large as ≈ 0.5 dex, particularly at $r \gtrsim 3r_{50}$.

j , but that is not as large as suggested by some of the idealised models (Romanowsky & Fall 2012).

We compare the mean radial j_{stars} profiles to the theoretical expectation of Mo et al. (1998) for a self-gravitating disk in a Navarro et al. (1997) dark matter profile in the bottom panel of Fig. 7. In this model, the halo is assumed to respond adiabatically to the assembly of the disk, and thus the AM of individual dark matter particles is conserved. No bulge component is included in this model. Mo et al. (1998) described the mean radial AM profile of disks as

$$J_d(< r) = \int_0^r V_c(R) R \Sigma(R) 2\pi R dR, \quad (4)$$

where $V_c(R) = \sqrt{GM/R}$, with $M = M_{\text{DM}}(R) + M_{\text{stars}}(R)$ being the stellar plus dark matter mass enclosed within R , and Σ the stellar surface density at R . Here we are implicitly neglecting the effect of the gas in the potential well of the galaxy, which makes sense as we are only analysing relatively massive galaxies, $10^{10.5} M_{\odot} \lesssim M_{\text{stars}} \lesssim 10^{11} M_{\odot}$, which have low gas fractions in EAGLE (Lagos et al. 2015; Crain et al. 2016).

We find that the subsample of galaxies that never suffered a merger follows the theoretical expectation of Mo et al. (1998) relatively closely, with a slightly steeper slope at $r \lesssim 2r_{50}$ and shallower at $r \gtrsim 4r_{50}$, reflecting the fact that these galaxies are not pure disks and that they do not follow precisely the assumption of exponential thin disks (e.g. Stevens et al. 2016b). This is consistent with the conclusion of Lagos et al. (2017) that EAGLE galaxies on average follow the expectation of isothermal collapsing halos

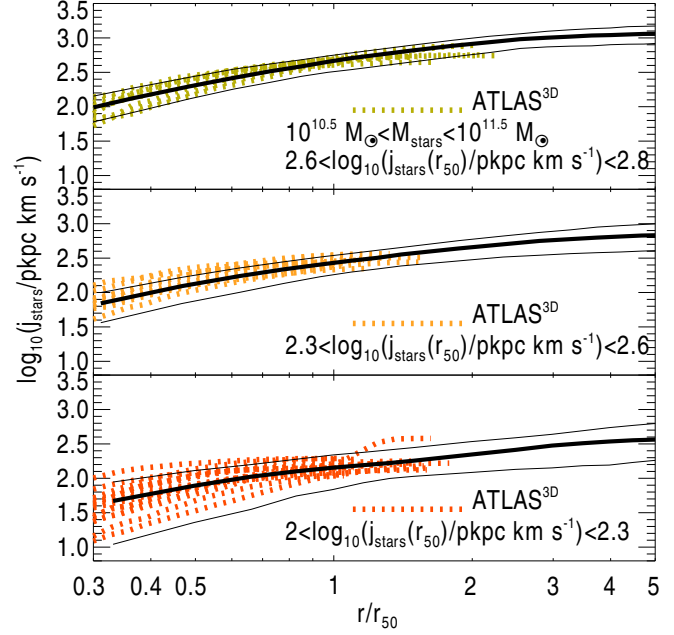


Figure 9. Mean radial j_{stars} profile for the same EAGLE galaxies of Fig. 8. For the simulated galaxies, we show the median and the 16th and 84th percentile ranges. Individual dotted lines show ATLAS^{3D} galaxies that have stellar masses in the range $10^{10.5} M_{\odot} - 10^{11.5} M_{\odot}$ and have $j_{\text{stars}}(r_{50})$ in the ranges shown in each panel. The agreement between EAGLE and the observations is excellent.

with weak conservation of AM (to within $\approx 50\%$; see their Fig. 15). However, the subsample of galaxies that had at least one dry merger significantly deviates from the theoretical prediction, with a j_{stars} that is on average lower by ≈ 0.6 dex and displaying a steeper increase with radii than that expected from Eq. 4. This is a consequence of significant losses of AM due the dissipative nature of mergers (e.g. Romanowsky & Fall 2012). We come back to this in § 4.

3.1.2 Comparison with observations of early-type galaxies

We compare EAGLE galaxies with low j_{stars} with the observations of Romanowsky & Fall (2012) in Fig. 8. Romanowsky & Fall (2012) presented mean radial j_{stars} profiles for 7 ellipticals and S0 galaxies in the stellar mass range of $10^{10.5} M_{\odot} \lesssim M_{\text{stars}} \lesssim 10^{11.5} M_{\odot}$. We took these 7 galaxies and separated them into 3 bins of $\log_{10}(j_{\text{stars}}(r_{50})/\text{pkpc km s}^{-1})$, 2 – 2.3, 2.4 – 2.6 and 2.6 – 2.8, which in EAGLE would correspond to galaxies below, close to and above the median $j_{\text{stars}}(r_{50})$ at that stellar mass, and compare them with EAGLE in Fig. 8. Note that in EAGLE most galaxies of such stellar mass are expected to be early-type (see Fig. 5). We find that at low j_{stars} (bottom panel of Fig. 8) the scatter in the mean radial profiles becomes increasingly larger compared to galaxies of higher j_{stars} , and galaxies with flat mean j_{stars} profiles become more common. EAGLE describes the variety of mean radial j_{stars} profiles observed by Romanowsky & Fall (2012) very well, even the cases where j_{stars} ceases to increase at $r \gtrsim 3r_{50}$.

With the aim of testing EAGLE with a larger number of galaxies, we extracted mean radial j_{stars} profiles for every ATLAS^{3D} galaxy (Cappellari et al. 2011), following the procedure described in Lagos et al. (2017). These profiles sample up to $\approx 2r_{50}$ in the best cases, but they inform us of the shape of the radial j_{stars} pro-

file in the inner regions of galaxies. Fig. 9 shows the comparison between EAGLE and ATLAS^{3D} in the same stellar mass and $j_{\text{stars}}(r_{50})$ ranges of Fig. 8. From top to bottom, each panel shows 8, 10 and 15 ATLAS^{3D} galaxies, respectively. The agreement with the observations is excellent. ATLAS^{3D} displays a trend of the scatter in the radial j_{stars} profiles increasing when going to low spin galaxies of a very similar magnitude to the one seen in EAGLE. This gives us confidence that the simulation not only reproduces the average j -mass relation, as shown by Lagos et al. (2017), but also the radial profiles of galaxies, where observations exist. The number of galaxies in the Universe in which this comparison can be done is still very sparse, but the advent of IFU instruments (e.g. SAMI, MaNGA, MUSE) is likely to change this.

3.2 j_{stars} before and after galaxy mergers

We analyse how much $j_{\text{stars}}(r_{50})$ changes between two consecutive snapshots for galaxies with $M_{\text{stars}} \geq 10^{9.5} M_{\odot}$ and in the redshift range $0 \leq z \leq 2.5$, separating galaxies into those that had and did not have a merger, and splitting mergers into different types: minor/major, wet/dry and with different spin alignments and orbital parameters. This is shown in the top panel of Fig. 10 (the equivalent for $j_{\text{stars}}(5r_{50})$ is shown in Fig. B1). The bottom panel of Fig. 10 shows the fraction that display an increase in $j_{\text{stars}}(r_{50})$ for the same cases analysed in the top panel. The first 3 data points compare the change in $j_{\text{stars}}(r_{50})$ due to smooth accretion and a minor or major merger. In the latter case, star formation and gas accretion may continue, and thus, we cannot fully separate the effect of the merger. Galaxies that did not suffer mergers on average increase their $j_{\text{stars}}(r_{50})$ by $\approx 15\%$ in between snapshots, and are likely to undergo an important increase in $j_{\text{stars}}(r_{50})$ (i.e. $\approx 35\%$ of the galaxies at least double their $j_{\text{stars}}(r_{50})$ in a snapshot). On the contrary, galaxy mergers are more likely to not change or reduce their $j_{\text{stars}}(r_{50})$, depending on whether they are minor or major mergers, respectively. From the bottom panel of Fig. 10, one sees that smooth accretion increases $j_{\text{stars}}(r_{50}) \approx 60\%$ of the time, while minor and major mergers only do this in $\approx 54\%$ and $\approx 43\%$ of the cases, respectively.

In § 3 we concluded that dry and wet mergers have very different net effects on j_{stars} , so in Fig. 10 we split mergers into several subsamples to pin down the circumstances in which j_{stars} decreases/increases the most. We first take all of the minor and major mergers and split them into dry and wet (shown from the 4th to the 7th symbols and bars in Fig. 10). We find that wet minor mergers produce a similar increase of $j_{\text{stars}}(r_{50})$ to smooth accretion, with a smaller percentage of galaxies going through a major increase in $j_{\text{stars}}(r_{50})$ ($\approx 20\%$ of wet minor mergers produce an increase of more than a factor of 2). Dry minor mergers, on the other hand, display a strong preference for decreasing $j_{\text{stars}}(r_{50})$. For major mergers the trends are similar but with a larger difference between dry and wet mergers. Dry major mergers reduce $j_{\text{stars}}(r_{50})$ in $\approx 75\%$ of the cases, which shows that this is one of the most catastrophic forms of mergers for the AM budget of galaxies. Note that in EAGLE *the gas fraction of the merger is more important than the mass ratio*. We calculate the Kolmogorov-Smirnov p -value between dry and wet mergers for the cases of minor and major mergers and find that there is negligible probability, $< 10^{-15}$, that they are drawn from the same population.

So far we have stacked all of the galaxy mergers that take place in galaxies with $M_{\text{stars}} \geq 10^{9.5} M_{\odot}$ and in the redshift range $0 \leq z \leq 2.5$. This may introduce significant biases due to the time interval between outputs of the simulation (different snap-

shots cover different timescales), and also due to galaxies having very different sizes at different cosmic epochs. In Appendix B we show that the bias introduced by studying mergers at different cosmic epochs and taking place in galaxies of different stellar masses is minimal, and that the difference seen here between minor/major, wet/dry mergers is of the same magnitude in subsamples at different redshifts and stellar masses. From here on, we analyse galaxy mergers together, regardless the cosmic epoch and the stellar mass of the galaxy in which they occur, unless otherwise stated.

Given the importance of wet/dry mergers over minor/major mergers, we explore the effect of spin alignments and orbital parameters in the subsamples of dry and wet mergers in the right part of Fig. 10. We first measure the effect of co-rotating ($\cos(\theta_{\text{spin}}) > 0.7$), perpendicular ($-0.15 < \cos(\theta_{\text{spin}}) < 0.15$) and counter-rotating ($\cos(\theta_{\text{spin}}) < -0.7$) mergers (middle symbols and bars in Fig. 10). We find that wet mergers between co-rotating galaxies lead to a larger and more frequent increase of $j_{\text{stars}}(r_{50})$, while perpendicular wet mergers tend to produce little changes in $j_{\text{stars}}(r_{50})$. 64% of the co-rotating dry minor mergers increase $j_{\text{stars}}(r_{50})$, a frequency that is even higher than smooth accretion. The effect of counter-rotating mergers is in between the co-rotating and perpendicular mergers. Perpendicular mergers are the most common configuration in EAGLE (see Fig. 2) and that is why the bars for wet minor and major mergers are weighted more heavily towards the results of perpendicular rather than to co-rotating mergers. For dry mergers we find the same trend: co-rotating mergers tend to be less damaging than perpendicular or counter-rotating mergers for $j_{\text{stars}}(r_{50})$.

In the rightmost part of Fig. 10 we analyse the effect of the orbital parameters. Particularly, we analyse co-planar and perpendicular mergers, the subsample with high j_{orbital} (i.e. higher than the median), and with high and low $j_{\text{orbital}}/j_{\text{stars}}(5r_{50})$ (above and below the median, respectively). § 2.1 presents the definition of j_{orbital} , and here we compare j_{orbital} to $j_{\text{stars}}(5r_{50})$ of the primary galaxy prior to the merger. $j_{\text{stars}}(5r_{50})$ is a good measurement of the galaxy's total j_{stars} (see Fig. 6). We do not find a strong effect of the orientation of the mergers on $j_{\text{stars}}(5r_{50})$, as both the distributions of the co-planar and perpendicular mergers are statistically indistinguishable (the KS p -value is 0.56). When comparing mergers of high and low j_{orbital} , we find a significant difference (with a KS p -value of 10^{-5}) in which mergers with high j_{orbital} preferentially result in an increase in $j_{\text{stars}}(5r_{50})$ of $\approx 15\%$. The largest systematic is found when we separate wet mergers by their $j_{\text{orbital}}/j_{\text{stars}}(5r_{50})$ (the p -value comparing the two subsamples of high/low $j_{\text{orbital}}/j_{\text{stars}}(5r_{50})$ is 10^{-24}). High values of $j_{\text{orbital}}/j_{\text{stars}}(5r_{50})$ efficiently spin-up the galaxy, increasing $j_{\text{stars}}(5r_{50})$ by $\approx 22\%$, on average, and in 60% of the cases. This suggests that galaxies spin-up because part of the orbital AM is transferred to the remnant galaxy. We study the subsample of wet, co-rotating ($\cos(\theta_{\text{spin}}) > 0.7$) and high $j_{\text{orbital}}/j_{\text{stars}}(5r_{50})$ mergers, and find that they increase $j_{\text{stars}}(5r_{50})$ in $\approx 70\%$ of the cases, by $\approx 44\%$ on average, and thus this form of merger is the most efficient at spinning-up galaxies. In the case of dry mergers we do not find a strong dependence on any of the orbital parameters studied here.

When studying $j_{\text{stars}}(5r_{50})$ (Fig. B2) we find very similar results. The only major difference is that dry mergers show a stronger dependence on the orbital parameters, with high $j_{\text{orbital}}/j_{\text{stars}}(5r_{50})$ and co-planar mergers leading to a higher fraction of galaxies displaying and increase in $j_{\text{stars}}(5r_{50})$. One could conclude that the AM in the inner parts of galaxies during dry mergers is not greatly affected by the orbital parameters of the

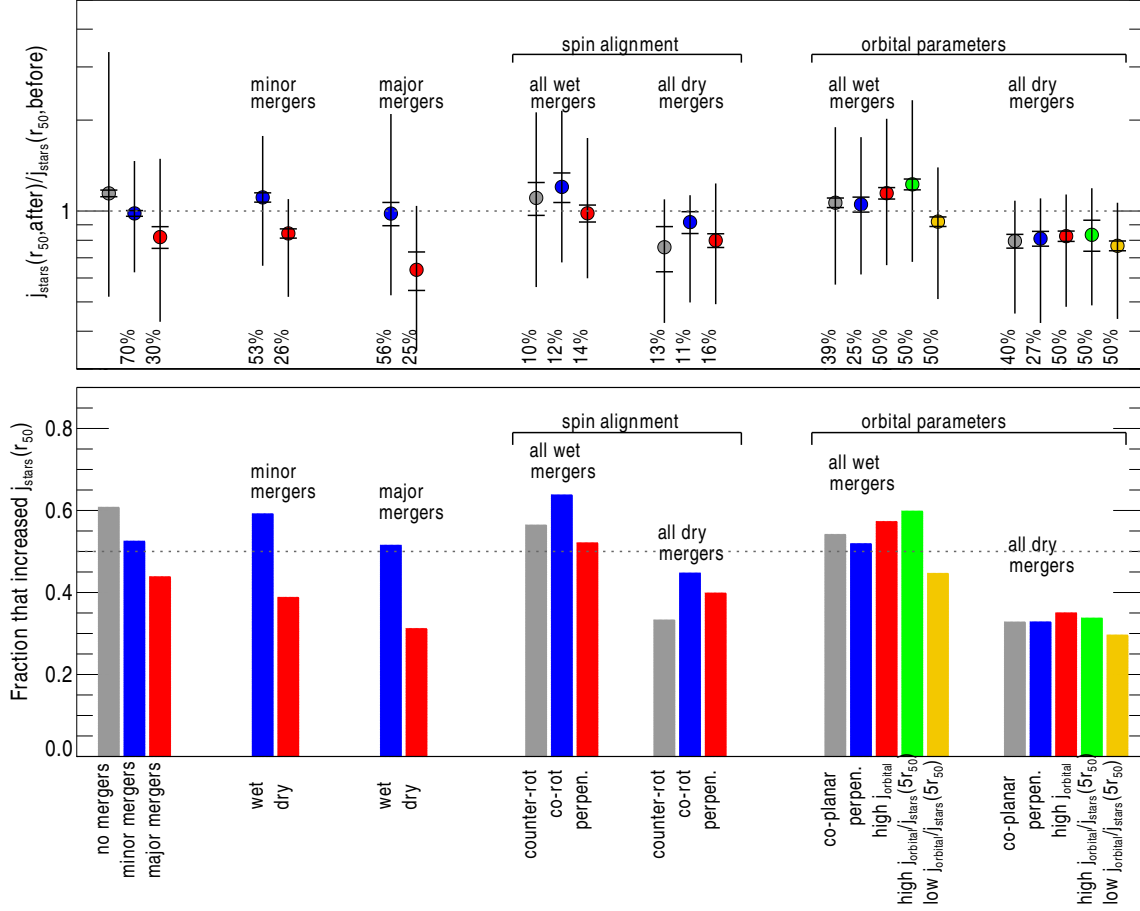


Figure 10. *Top panel:* the ratio of $j_{\text{stars}}(r_{50})$ in a galaxy between two consecutive snapshots. We separate galaxies into those that had no mergers, and those that went through a minor or a major merger (first 3 symbols); galaxies that went through a minor or major merger, separated into wet and dry (subsequent 4 symbols); galaxies that went through wet and dry mergers separated into three samples of spin alignment (counter-rotating, co-rotating and perpendicular, as defined in § 2; subsequent 6 symbols), and separated into 5 orbital parameter samples (co-planar and perpendicular mergers, and mergers with high orbital AM, and high/low orbital-to-central galaxy AM; subsequent 10 symbols), as labelled in the x -axis. The symbols show the medians, while the small and large errorbars show the statistical uncertainty on the median (from bootstrap resampling) and the 25th – 75th percentile ranges, respectively. The dotted line shows no change in $j_{\text{stars}}(r_{50})$. At the bottom of the panel we show the percentage of the mergers that are included in each subsample. *Bottom panel:* Fraction of galaxies that display an increase in their $j_{\text{stars}}(r_{50})$ in the same cases shown for the same selections of the top panel. For reference, the dotted line shows a fraction of 0.5. We find that on average galaxy mergers have a negative effect on $j_{\text{stars}}(r_{50})$, as a smaller fraction leads to an increase in $j_{\text{stars}}(r_{50})$ compared to smooth accretion. However, the nature of the merger has a large effect on the outcome: wet, co-rotating mergers tend to increase $j_{\text{stars}}(r_{50})$, while dry, counter-rotating mergers have the most negative effect on $j_{\text{stars}}(r_{50})$.

mergers, but when focusing on the total j_{stars} , we see that perpendicular and low $j_{\text{orbital}}/j_{\text{stars}}(5r_{50})$ mergers, are the most catastrophic.

We conclude that in EAGLE wet, co-rotating mergers can spin-up galaxies very efficiently, and even more if they have a high $j_{\text{orbital}}/j_{\text{stars}}(5r_{50})$. On the contrary, dry, counter-rotating mergers are the most effective at spinning down galaxies. The environment in which these mergers take place may have a significant impact. We find that wet mergers generally happen in halos of higher spins compared to the median of all halos. This could be interpreted as accretion spinning up halos, as well as making the galaxies gas-rich and resulting in a high spin merger remnant. The consequences of a such correlation are very interesting but beyond the scope of this paper, so we defer it to future investigation.

3.3 Rearrangement of j_{stars} during galaxy mergers

In Fig. 11 we study the mean radial j_{stars} profile of the primary galaxy before and after the merger in two bins of stellar mass and for minor/major mergers that are wet/dry. *Before* the merger here means the last snapshot in which the galaxy participating in the merger was individually identified, and for ‘*after*’ the merger we look at the two consecutive snapshots in which the galaxies has been identified as one (i.e. already merged in the merger tree). Given the time period in between snapshots, the two consecutive snapshots roughly correspond to ≈ 0.5 Gyr and ≈ 1 Gyr, respectively, after the merger. We study two snapshots after the merger as visual inspection of mergers in EAGLE quickly reveals that in some cases SUBFIND considers a galaxy pair as already merged even though the process is still ongoing. We show in Fig. 12 an example of a wet minor merger that takes place between the snapshots $z = 0.503$ and $z = 0.366$, but it is clear that although the galaxy pair is considered as merged in snapshot $z = 0.366$, in

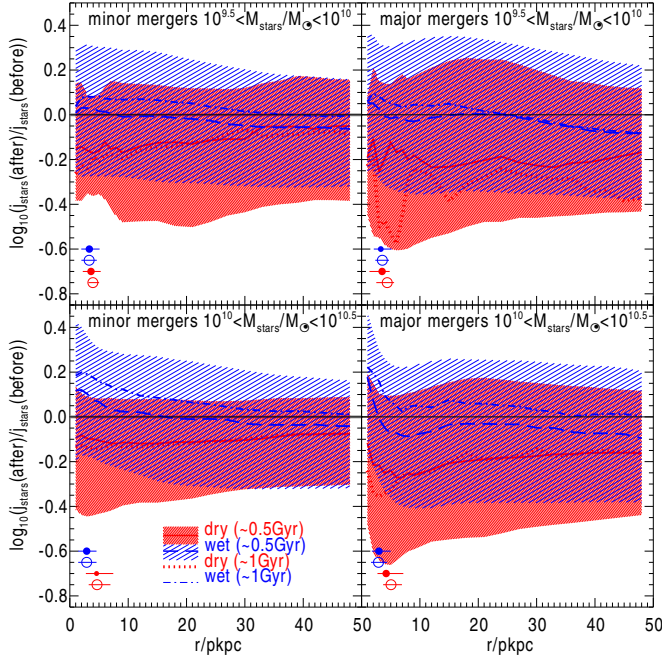


Figure 11. The ratio between the mean radial j_{stars} profiles after and before the galaxy merger, measured in an aperture r , as a function of r . We measure j_{stars} post-merger in the snapshot right after the merger, and two snapshots after, which correspond approximately to 0.5 and 1 Gyr after the merger, respectively. Minor and major mergers are shown in the left and right panels, respectively, in two bins of the neutral gas fraction of the merger, as labelled. The top panels show galaxies with $10^{9.5} M_{\odot} < M_{\text{stars}} < 10^{10} M_{\odot}$, while the bottom panels show galaxies with $10^{10} M_{\odot} < M_{\text{stars}} < 10^{10.5} M_{\odot}$. Lines and the shaded regions show the median and the 25th-75th percentile ranges. The latter are calculated using the snapshots right after the merger. The filled and empty circles with the error bar at the bottom of each panel show the median r_{50} before and after the merger, respectively, for each sample and the 25th-75th percentile range, respectively. The figure reveals how gas-rich mergers tend to increase j_{stars} in the inner regions of galaxies, while decreasing it in the outer regions. Horizontal lines mark no change in $j_{\text{stars}}(r)$, and so values above the line show an increase in j_{stars} , while the opposite holds if below the line.

reality they have only had a first passage, and which is only complete at $z = 0.271$, which is the next snapshot. This figure shows maps of the atomic and molecular column densities (calculation is described in Lagos et al. 2015), and stellar density of the galaxy merger in the three snapshots above. We also show here the SDSS gri synthetic images of the primary galaxy in the three snapshots, in the same viewing angle used for the gas and stellar maps. In this example, one nicely sees the effect of gas compression produced by the mergers in the collision front enhancing the column densities of both HI and H₂ (clear in the middle panel of Fig. 12, once the galaxies had a first passage). By $z = 0.271$ the galaxy pair had finished merging. Cases like Fig. 12 are more common in gas-rich than in gas-poor mergers.

In addition to cases such as the one shown in Fig. 12, we study two consecutive snapshots after the merger to study the effect of relaxation if any is present. In the low stellar mass bin of Fig. 11, we show that both dry minor and major mergers have the effect of reducing j_{stars} across the entire radii range considered. Studying j_{stars} at ≈ 0.5 or ≈ 1 Gyr after the merger makes little difference in this case. Major dry mergers tend to reduce j_{stars} by ≈ 0.2 dex on average in both low and high stellar mass bins, while minor dry

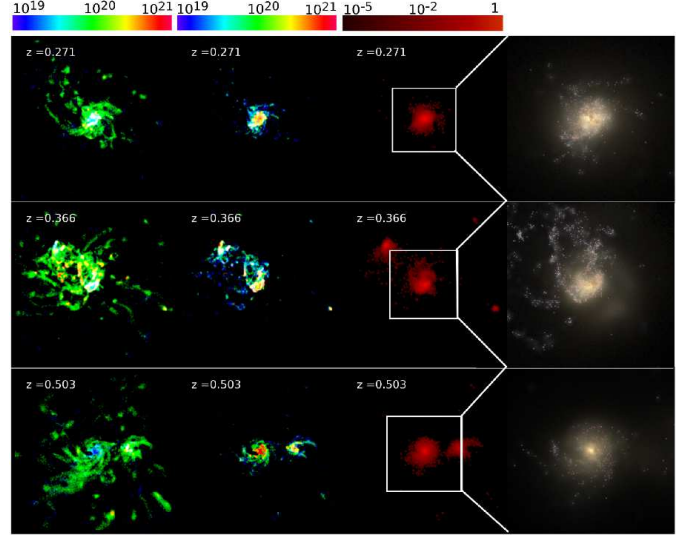


Figure 12. Example of a gas-rich minor merger that at $z = 0.503$ is identified as two separate galaxies, and at $z = 0.366$ as one galaxy, although it has not finished merging. By $z = 0.271$ the galaxy already appears as merged. The first three columns of images are 0.2 cMpc on a side, while the right-hand column shows synthetic g, r, i optical images that are 60 kpc on a side. The latter are images of the central, more massive galaxy and are publicly available from the EAGLE database (McAlpine et al. 2015). Images are viewed down the z -axis, and thus their horizontal and vertical axis correspond to the simulation x and y -axis, respectively. The panels from left to right show HI and H₂ column densities (in units of cm^{-2}), stellar density (in units of M_{\odot}/pc^3), and optical images respectively, as marked by the colour bars at the top. Cases like this are more common in gas-rich mergers rather than gas poor mergers, and thus it is necessary to analyse the galaxy remnant two snapshots after the merger to get a more accurate measurement of the AM of the galaxy.

mergers drive a more modest reduction of ≈ 0.1 dex, on average. In the case of wet mergers we see a differential effect on the j_{stars} profiles: inner regions of galaxies, $r \lesssim 5$ kpc (typically $\approx 2r_{50}$; see filled and open circles in Fig. 11), tend to increase j_{stars} , while at larger radii j_{stars} tends to decrease if one looks at the merger remnant ≈ 0.5 Gyr after the merger, or very modestly increase if studied ≈ 1 Gyr after. The latter could be due to a combination of relaxation and continuing gas accretion and star formation. Separating the latter is not obvious in a simulation like EAGLE where all the physical processes are interplaying at any given time.

3.3.1 The physical origin of the j_{stars} increase in wet mergers

To further understand the differential effect wet mergers have on the mean radial j_{stars} profile, we study in Fig. 13 the change in the stellar surface density of the primary galaxy before and after the merger. For clarity, we only plot the mass bin $10^{10} M_{\odot} < M_{\text{stars}} < 10^{10.5} M_{\odot}$ as the lower mass bin gives very similar results. Fig. 13 shows that wet major and minor mergers drive a significant increase in the central stellar surface density by a factor $\gtrsim 0.2$ dex, on average. At intermediate radii, $5 \text{ pkpc} \lesssim r \lesssim 30 \text{ pkpc}$ there is also an increase, but of a less significant magnitude. If the central stellar mass (i.e. bulge) is increasing, and the rotational velocity increases as $v = \sqrt{GM/r}$, j_{stars} is also expected to increase. This effect has been seen before in non-cosmological simulations of gas-rich mergers (Springel 2000; Cox et al. 2006;

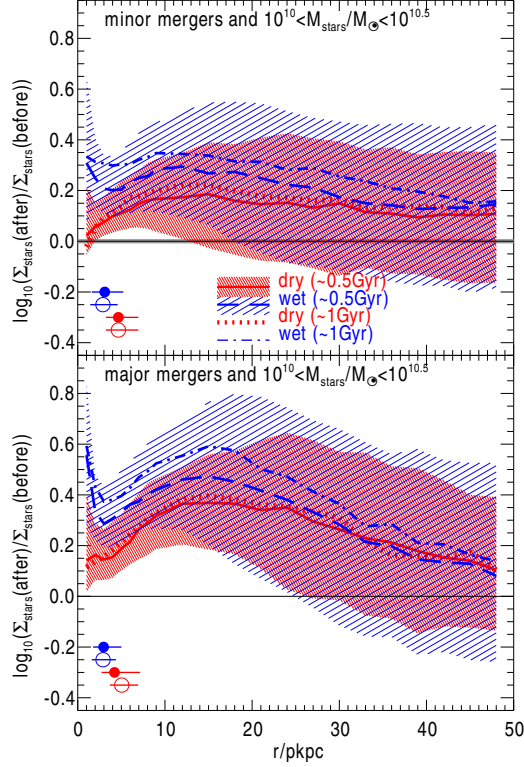


Figure 13. Stellar mass surface density profile before and after the mergers for the galaxies in the bottom panel of Fig. 11. This figure shows that gas-rich mergers tend to build the central stellar mass concentration (i.e. bulge), while dry mergers increase the stellar mass density towards the outskirts of galaxies. the latter case usually drives an increase in r_{50} , while the former does not change r_{50} significantly.

Robertson et al. 2006; Johansson et al. 2009; Peirani et al. 2010; Moreno et al. 2015).

One remaining question is whether the build-up of the bulge is driven by a preferential deposition of the stars of the satellite galaxy in the centre, by dynamical friction moving stars of the primary galaxy to the centre, or the preferential formation of new stars in the centre. To answer this question we identified in the merger remnant the stars that belonged to the secondary (i.e. progenitor satellite stars) and primary (i.e. progenitor central stars) galaxy before the merger, and those that formed during the merger (i.e. new stars), and calculate their 50% and 90% stellar mass radii. We do this for all mergers that took place in the redshift range $\approx 0.2-0.8$, which is of particular interest, as it is the time when the universe goes from being dominated by wet to dry mergers in EAGLE (see Fig. 2). Fig. 14 shows the ratio of r_{50} and r_{90} between the progenitor satellite stars and the progenitor central stars, and between the new stars and the progenitor central stars in the case of wet minor mergers. For the new stars, we find that in $\approx 73\%$ of cases they end up more concentrated and with r_{50} and r_{90} typically ≈ 1.3 times smaller than the progenitor central stars. For the progenitor satellite stars, we find that in $\approx 70\%$ of the cases they end up more extended and with r_{50} and r_{90} values that are ≈ 1.8 and ≈ 1.3 times larger than those of the progenitor central stars. The bottom panel of Fig. 14 shows 4 examples of wet minor merger remnants and how the progenitor satellite, central and newly formed stars are spatially distributed. We generally find that when r_{50} of the progenitor satellite stars is larger than that of the progenitor central

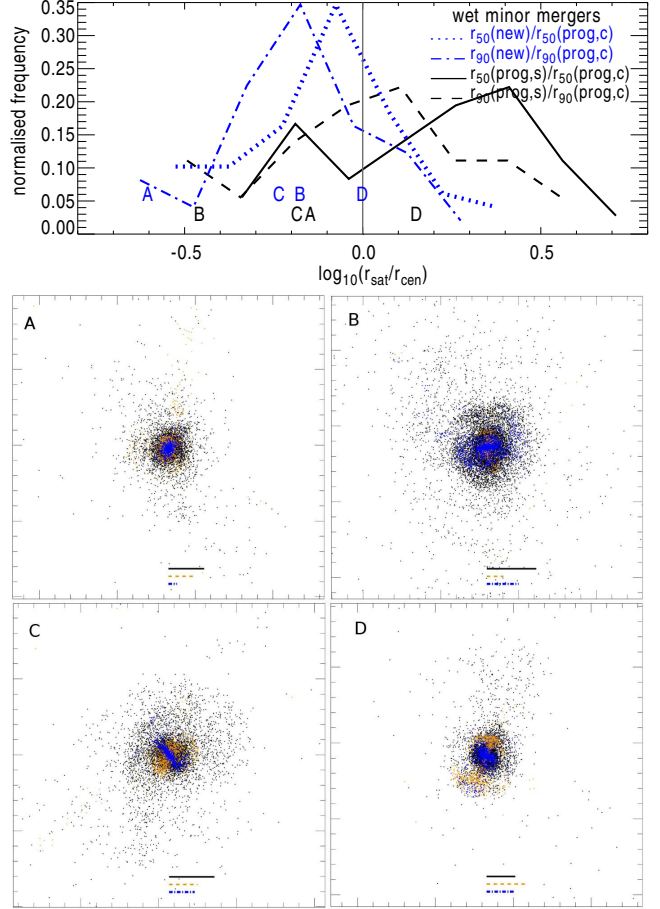


Figure 14. *Top panel:* The ratio between the 50% and 90% stellar mass radii of the progenitor satellite (labelled as ‘prog.s’) and the newly formed stars (labelled as ‘prog.c’) components, as labelled, in all wet minor mergers in the redshift range $\approx 0.2-0.8$ and that took place in primary galaxies with $M_{\text{stars}} \geq 10^{9.5} M_{\odot}$ in EAGLE. This figure shows that newly formed stars reside in the centre of the galaxy, and are more concentrated than the stars that were in primary galaxy before the merger. Progenitor satellite stars also end up preferentially more concentrated than the progenitor stars of the primary galaxies but to a lesser degree when compared to newly formed stars. *Bottom panel:* stellar-particle distribution in 4 examples of wet major mergers that span the range of size ratios shown in the top panel. The images are x - y projections of 200 kpc on a side. Black, yellow and blue points show progenitor stars that belonged to the primary galaxy, progenitor stars that belonged to the secondary galaxy and stars that formed during the merger, respectively. The segments of the same colours at the bottom show r_{90} of the three components.

stars there is an associated extended stellar structure in the form of streams or shells (e.g. galaxy ‘D’ in Fig. 14). If we focus on the central 2 pkpc, we find that the bulge mass is dominated by the progenitor central stars ($\approx 70\%$ on average), but with a large contribution from the newly formed stars ($\approx 30\%$ on average). Although there is a significant contribution of newly formed stars, we find that the mass-weighted age of the bulge by $z = 0$ is $\gtrsim 9.5$ Gyr old, on average, due to the stars contributed by the primary and secondary galaxies that end up in the central 2 pkpc being extremely old.

We also studied the contribution of these stars to the mean \dot{j}_{stars} radial profile of the merger remnant in the inner 20 pkpc in

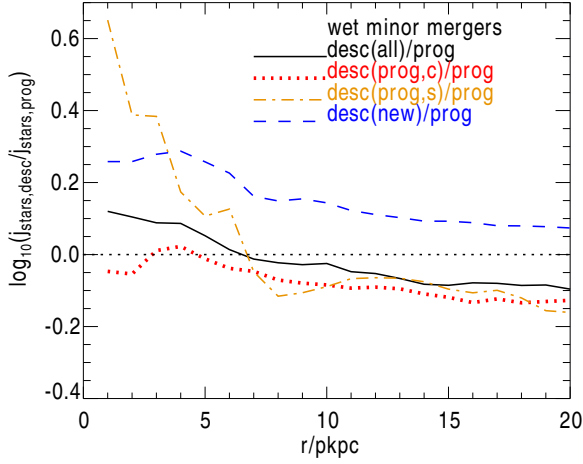


Figure 15. The ratio between the mean radial j_{stars} profiles after and before the galaxy merger (solid line), measured in an aperture r , as a function of r , for all wet minor mergers in the redshift range $\approx 0.2 - 0.8$ and that took place in primary galaxies with $M_{\text{stars}} \geq 10^{9.5} M_{\odot}$ in EAGLE. We also show the ratio between the mean radial j_{stars} profiles of the descendant and the progenitor but when we measure the former only with the progenitor central (dotted line), progenitor satellite (dot-dashed line) and newly formed stars (dashed line). Here lines show the medians. The increase seen in j_{stars} in $r \lesssim 5$ pkpc as a result of the merger is similar to that shown in Fig. 11, but here we show that the increase is due to the contribution of newly formed stars (which make a substantial contribution to the stellar mass). Although the progenitor satellite stars also have a large j_{stars} in the centre, their contribution to the stellar mass is negligible.

Fig. 15. We find that the increase in j_{stars} in the inner regions of galaxies as a result of the wet merger and reported in Fig. 11 is due to the newly formed stars. Although the progenitor satellite stars also have a high j_{stars} compared to the progenitor central stars, their contribution to the stellar mass is very small. In fact, in the inner 3 pkpc, newly formed stars are responsible for 33% of the j_{stars} of the descendant, while progenitor central and satellite stars contribute 58% and 9%, respectively, on average. At larger radii, j_{stars} of the descendant becomes more dominated by the stars of the progenitor central galaxy.

The main difference between wet minor and major mergers, is that in the latter (not shown here) the stars belonging to the progenitor secondary (or satellite) galaxy end up more concentrated than the progenitor central stars (typically ≈ 1.5 times more concentrated, on average). The other results shown in Fig. 14 hold for wet major mergers.

We conclude that the increase of j_{stars} in the inner regions of galaxies as a result of a wet merger is caused primarily by the flows of gas towards the centre that subsequently form stars. These new stars contribute to the formation of the bulge, that deepens the potential well and produces a steeper velocity profile (with the rotational velocity growing as $\sim \sqrt{GM/r}$).

3.3.2 Stellar mass deposition during dry mergers

We now return to the case of dry mergers in Fig. 11 and 13. Despite the increase in stellar mass surface density at intermediate radii ($10 \text{ pkpc} \lesssim r \lesssim 40 \text{ pkpc}$), we obtain a significant decrease of j_{stars} . We analyse the structures formed by the progenitor central and satellite galaxies, and the newly formed stars if any are

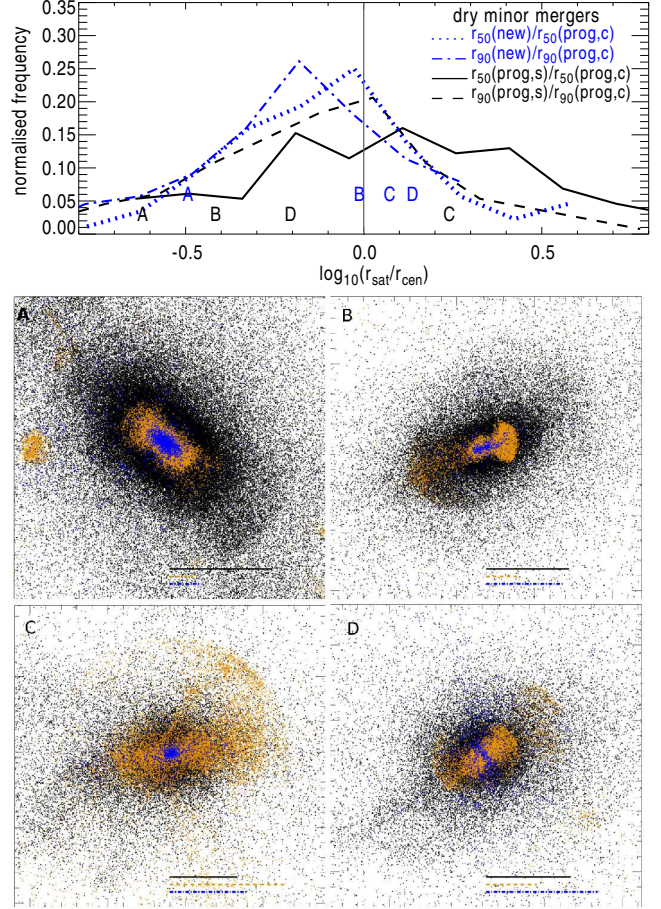


Figure 16. As Fig. 14 but for dry minor mergers.

present. We remind the reader that dry here is not strictly devoid of gas, but simply gas poor, and thus, some star formation can take place during dry mergers. Fig. 16 shows the ratio of r_{50} and r_{90} between the progenitor satellite stars and the progenitor central stars, and between the new stars and the progenitor central stars for all dry minor mergers that took place between $0.2 \lesssim z \lesssim 0.8$ in galaxies with $M_{\text{stars}} \geq 10^{9.5} M_{\odot}$ in EAGLE. We again find that, if any star formation takes place, those stars preferentially reside in the centre due to the efficient transport of the gas to the central regions. This is similar to what is seen in observations as molecular and atomic hydrogen disks and dust lanes in early-type galaxies, which are thought to be the result of minor mergers with gas-rich dwarf galaxies (e.g. Davis et al. 2015). If r_{50} of the new stars is larger than the progenitor central stars, it is usually because there are very few newly formed stars, and thus the measurement of r_{50} is noise-dominated. We study the stellar mass budget in the intermediate radii range above, and find that the increase in Σ_{stars} shown in Fig. 13 is consistent with how much mass from the progenitor satellite stars is deposited at these radii ($\approx 20\%$ of the stellar mass budget at $10 \text{ pkpc} \lesssim r \lesssim 40 \text{ pkpc}$ comes from progenitor satellite stars). Such stars are also being deposited preferentially at larger radii than where the progenitor central stars reside (this is seen as larger r_{50} and r_{90} of the progenitor satellite stars compared to the progenitor central stars in Fig. 16). This is consistent with what simulations of dry minor mergers have found (e.g. Taranu et al.

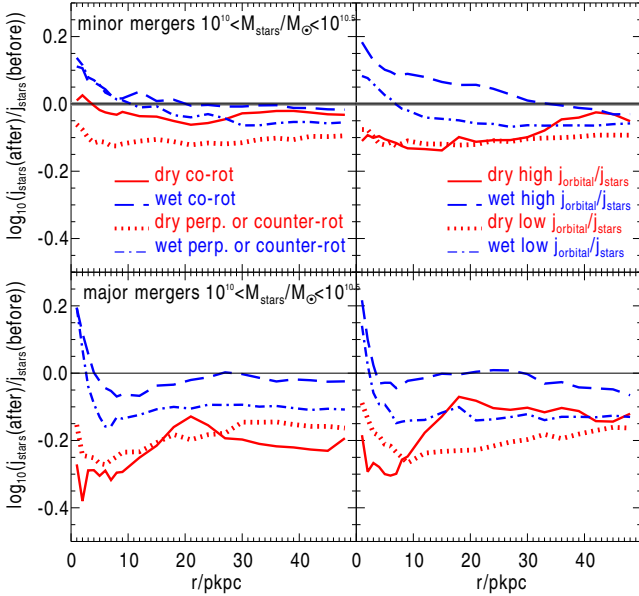


Figure 17. The ratio between the mean radial j_{stars} profiles after and before the galaxy merger, measured in an aperture r , as a function of r for galaxies with stellar masses in the range $10^{10} M_{\odot} < M_{\text{stars}} < 10^{10.5} M_{\odot}$ at $z < 2$. Mergers are split into minor (top panels) and major (bottom panels). In addition, every panel shows wet and dry mergers as red and blue lines split into co-rotating vs. perpendicular or counter-rotating mergers (left panels), high vs. low $j_{\text{orbital}}/j_{\text{stars}}$ (right panels), as labelled. Here we study consecutive snapshots, which in practice means that the profile *after* the merger is measured at $\approx 0.3 - 0.5$ Gyr after the merger. Lines correspond to the medians of the distributions. For clarity we do not show here the percentile ranges, but they are of a similar magnitude to those shown in Fig. 11. This figure shows that dry major mergers always have a catastrophic consequence on the j_{stars} profile regardless of the spin alignments and orbital parameters, while in the case of dry minor mergers we find that they all cause a decrease in j_{stars} except if the merger happens in galaxies with spins highly aligned. In the case of wet minor and major mergers, co-rotating galaxies, and configurations with high $j_{\text{orbital}}/j_{\text{stars}}$ ratio lead to a more significant increase of j_{stars} in the centre, and smaller changes at large radii.

2013). The examples given in Fig. 16 show how such progenitor satellite stars can form shells that are responsible for increasing Σ_{stars} at intermediate and large radii.

In the case of dry major mergers (not shown here), we find that newly formed stars (though a very small fraction) they contribute to the central stellar surface density as in Fig. 16. Progenitor satellite stars typically end up more compact than the progenitor central stars (the difference here is similar to those found between wet minor and major mergers). When extended configurations are seen for the progenitor satellite stars they are typically in the form of shells. We find that at intermediate radii, $10 \text{ pkpc} \lesssim r \lesssim 40 \text{ pkpc}$, progenitor satellite stars contribute $\approx 30 - 50\%$, explaining partially the increase seen in Σ_{stars} at those radii in Fig. 13.

3.3.3 The effect of spin and orbital alignments

From Fig. 10 we concluded that in EAGLE wet, co-rotating mergers can spin-up galaxies very efficiently, while dry, counter-rotating mergers are the most effective at spinning down galaxies. In Fig. 17 we show the mean radial j_{stars} profiles of galaxies before and after the merger. After the merger here means the first time output in

which the two merging galaxies are identified as one single remnant (typically 0.5 Gyr after the merger). In the left panels of Fig. 17 we separate dry and wet minor (top) and major (bottom) mergers that took place in galaxies with $10^{10} M_{\odot} < M_{\text{stars}} < 10^{10.5} M_{\odot}$ into the subsamples of co-rotating ($\cos(\theta_{\text{spin}}) > 0.7$; see Eq. 2 for a definition of θ_{spin}), and perpendicular or counter-rotating galaxies ($\cos(\theta_{\text{spin}}) < 0.15$).

Wet minor mergers of galaxies that are co-rotating spin up the central region, due to the build-up of the bulge, and have very little effect on the outskirts of the galaxy (i.e. $j_{\text{stars}}(\text{after}) \sim j_{\text{stars}}(\text{before})$). In the case of perpendicular or counter-rotating galaxies, there is a significant spin down at $r \gtrsim 10 \text{ pkpc}$ of $\approx 40\%$, on average, as a result of a major merger, and a more modest one of $\approx 12\%$ in the case of minor mergers. A very significant difference is seen in dry minor mergers between co-rotating or perpendicular/counter-rotating galaxies. We find that very little happens to $j_{\text{stars}}(r)$ if the dry minor merger is between co-rotating galaxies, while in the case of perpendicular/counter-rotating mergers, there is a significant stripping of $j_{\text{stars}}(r)$ of $\approx 30\%$, on average, through the entire radii range studied here. Note that in the case of dry major mergers, there is always a significant stripping of j_{stars} regardless of the spin and orbital parameters.

In the right panels of Fig. 17 we show the ratio between the mean radial j_{stars} profiles before and after the merger as a function of r for subsamples of dry/wet minor/major mergers, split into two bins of $j_{\text{orbital}}/j_{\text{stars}}(5r_{50})$. These two bins are above (high $j_{\text{orbital}}/j_{\text{stars}}(5r_{50})$) and below (low $j_{\text{orbital}}/j_{\text{stars}}(5r_{50})$) the median value of $j_{\text{orbital}}/j_{\text{stars}}(5r_{50})$. Here $j_{\text{stars}}(5r_{50})$ corresponds to the value of the primary galaxy prior to the merger. In § 3.2 we show that this was the most important orbital parameter determining whether a galaxy suffered a spin up or down as a result of the merger. In the case of high $j_{\text{orbital}}/j_{\text{stars}}(5r_{50})$ we find that wet minor mergers result in a spin up that is significant all the way to $r \approx 30 \text{ pkpc}$, increasing $j_{\text{stars}}(r)$ by $\approx 60\%$ at $r \lesssim 5 \text{ pkpc}$ and $\approx 25\%$ at $5 \text{ pkpc} \lesssim r \lesssim 15 \text{ pkpc}$. Such a merger in EAGLE is the most effective at spinning up galaxies. These galaxies can end up in the upper envelope of the $j_{\text{stars}} - M_{\text{stars}}$ relation. For wet major mergers, we find a significant increase in the very inner regions ($r \lesssim 3 \text{ pkpc}$), and very little change at larger radii (i.e. $j_{\text{stars}}(\text{after}) \sim j_{\text{stars}}(\text{before})$). Dry mergers show very little difference between high and low $j_{\text{orbital}}/j_{\text{stars}}(5r_{50})$, on average. Di Matteo et al. (2009) showed that in the case of very high j_{orbital} the remnant can end up with a large j_{stars} even in the case of dry mergers. EAGLE reveals that this type of event is very rare, and most of the time the galaxies spin down as a result of a dry merger.

In the case of low $j_{\text{orbital}}/j_{\text{stars}}(5r_{50})$, wet minor and major mergers show modest to large losses of $j_{\text{stars}}(< r)$ of $\approx 15\%$ and $\approx 35\%$, respectively, on average. This large difference between the high/low $j_{\text{orbital}}/j_{\text{stars}}(5r_{50})$ subsamples arise from the efficient transfer of j_{orbital} onto the remnant galaxy, which can significantly spin up a galaxy when j_{orbital} is large.

4 DISCUSSION AND CONCLUSIONS

The classic interpretation of the positions of spiral and elliptical galaxies in the $j_{\text{stars}} - M_{\text{stars}}$ plane by e.g. Fall (1983) and Romanowsky & Fall (2012) has been that spiral galaxies are the result of weak conservation of specific AM of the gas falling in and forming stars, while elliptical galaxies have have lost $\gtrsim 50 - 90\%$ of their j in the formation process. The preferred invoked mechanism responsible for such loss is galaxy mergers. However, using

EAGLE we find that this simple interpretation of the observations is full of caveats.

Stevens et al. (2016b) showed that in spiral, star-forming galaxies the cooling gas typically losses $\approx 50\%$ to $\approx 90\%$ of its specific AM (see their Fig. 10), but that the resulting high absolute value of j_{stars} (that effectively ends up being close to the specific AM of the halo) arose because the original specific AM started out significantly higher than that of the halo. Danovich et al. (2015) showed similar results using cosmological zoom-in simulations of massive galaxies. The net effect of the mechanisms above is that the galaxy disk in the case of spiral galaxies ends up with $j_{\text{stars}} \sim 0.4 j_{\text{halo}}$ to within 50% (Zavala et al. 2016; Lagos et al. 2017), which would indicate that weak conservation of AM is in place. The mechanisms in the detail appear to be a lot more complex and non-linear than the classic picture above, which inevitably opens the question: to what extent are we forcing $j_{\text{stars}} \sim j_{\text{halo}}$ in spiral galaxies through the process of tuning free-parameters in the model? Crain et al. (2015) showed that EAGLE needed some careful modelling and tuning of parameters of stellar feedback to ensure that the half-mass sizes of star-forming galaxies agreed reasonably well with observations. A consequence of such tuning may well result in this conspiracy of gas having a large j but then losing significant amounts of it while cooling, so that by $z = 0$ spiral galaxies have specific AM of the same magnitude as its halo. A possible solution for this conundrum is to perform detailed, high-resolution simulations of individual spiral galaxies in a cosmological context and test widely different feedback mechanisms with the aim of understanding which conditions lead to $j_{\text{stars}} \sim j_{\text{halo}}$ and how independent the tuning of parameters is of the evolution of specific AM.

While we find mergers to preferentially spin galaxies down, their influence can be quite varied, and in many cases they spin galaxies up significantly, positioning them in the upper envelope of the j_{stars} -stellar mass relation. This is the case of wet mergers between co-rotating galaxies and with high j_{orbital} relative to the j_{stars} of the galaxies prior to the merger. When studying the correlation of the position of galaxies in the j_{stars} -stellar mass plane and their merger history, we find the wet merger rate increases with decreasing stellar mass and increasing j_{stars} , while the dry merger rate increases with increasing stellar mass and decreasing j_{stars} . In fact, EAGLE shows that for the j_{stars} value of the merger remnant galaxy, the most important parameter is the gas fraction of the merger, rather than the mass ratio or the spin/orbital parameters. The latter play a secondary, nonetheless relatively important, role. Dry mergers are the most effective way of spinning down galaxies, though the subsample of minor, co-rotating mergers are relatively harmless. Counter-rotating dry mergers are the most efficient at spinning down galaxies. Here our working definition of wet and dry is very gas-rich and gas-poor, and thus dry mergers can have some gas involved ($f_{\text{gas,merger}} \approx 0.02$, on average for dry mergers). Thus, dry mergers may be slightly different than the purely collisionless experiments widely discussed in the literature (e.g. Boylan-Kolchin et al. 2005; Naab et al. 2006b; Taranu et al. 2013; Naab et al. 2014).

Classical results of dry mergers by early works (e.g. Barnes & Efstathiou 1987 and Navarro et al. 1997), show that dynamical friction redistributes j_{stars} in a way such that most of it ends up at very large radii, but if integrating over a large enough baseline, one would find j_{stars} converges to j_{halo} . These results were refuted by the observations of elliptical galaxies compiled by Romanowsky & Fall (2012); these authors showed in a sample of 7 early-type galaxies that some of them converged in their j_{stars} to

values that would indicate a large deficiency compared to an average j_{halo} . Using EAGLE we found that dry merger remnants have most of their j_{stars} budget at $r \gtrsim 5 \times r_{50}$, in agreement with the early works discussed above, but that the variety of the radial j_{stars} profiles of galaxies, particularly at low $j_{\text{stars}}(r_{50})$, can easily explain the rotation curves presented in Romanowsky & Fall (2012). We compared the EAGLE j_{stars} profiles with ATLAS^{3D} galaxies and also here found excellent agreement. The main difference between what we find with EAGLE and the early papers above, is that the total j_{stars} in the case of dry merger remnants converges to $\approx 20\%$ of the halo j , on average, while galaxies that never had a merger of the same stellar mass, typically have a total j_{stars} that is $\approx 40\%$ their j_{halo} . Thus, a relatively modest but significant difference is found between these two samples.

The case of wet mergers in EAGLE is very interesting from the perspective of j_{stars} and the morphology of galaxies. We find that in most of these mergers, the inner regions of galaxies undergo a spin up as a result of stars being formed in the central $\approx 2 - 5$ kpc with high circular velocities. These newly formed stars are the result of gas inflows triggered by the merger, and drive the build-up of the bulge. These new stars display a significantly more concentrated distribution compared to the stars that were present in the primary or the secondary galaxy before the merger. Stars that belonged to the secondary galaxy end up preferentially more concentrated than the stars of the primary galaxy in the case of major mergers, and significantly more extended in the case of minor mergers. These extended structures are in the form of streams and/or shells.

Key observational tests to support our findings for the effect of mergers on the j_{stars} of elliptical galaxies would be to increase the sample of elliptical galaxies with good kinematic information out to $10 r_{50}$. Our predictions are: (i) the mean radial j_{stars} profiles of ellipticals are typically shallower than spiral galaxies, and that (ii) these profiles continue to rise well beyond $10 r_{50}$. A cautionary note: many of these stars that are beyond $10 r_{50}$ would not necessarily be considered part of the galaxy, but instead they may belong to the stellar halo. In terms of the mean radial j_{stars} profile, however, we do not see obvious features that would indicate distinct stellar components.

A plausible strategy to test the raising j_{stars} profiles of ellipticals would be to use integral field unit surveys, such as SAMI and MaNGA, to define a suitable sample of galaxies, selected from the j_{stars} -stellar mass plane, with j_{stars} here measured within some relatively small aperture (e.g. SAMI used one effective radius to measure j_{stars} within; Cortese et al. 2016), and follow up to measure j_{stars} out to radii $> 10 r_{50}$. The latter can be achieved by studying the kinematics of planetary nebulae and/or globular clusters in elliptical galaxies (e.g. Coccato et al. 2009; Romanowsky et al. 2009; McNeil et al. 2010; Foster et al. 2011). In addition, the lack of information on the 3D stellar densities and velocities makes it necessary to develop fitting tools that enable the reconstruction of 3D galaxies by imposing Newtonian constraints on IFU data. Observations and modelling tools like the ones described here would provide stringent constraints to the simulation and the galaxy formation physics included in it.

ACKNOWLEDGEMENTS

We thank Luca Cortese and Matthieu Schaller for useful discussions and comments on the manuscript. CL is funded by a Discovery Early Career Researcher Award (DE150100618). CL also thanks the MERAC Foundation for a Postdoctoral Research Award.

This work was supported by a Research Collaboration Award at the University of Western Australia. This work used the DiRAC Data Centric system at Durham University, operated by the Institute for Computational Cosmology on behalf of the STFC DiRAC HPC Facility (www.dirac.ac.uk). This equipment was funded by BIS National E-infrastructure capital grant ST/K00042X/1, STFC capital grant ST/H008519/1, and STFC DiRAC Operations grant ST/K003267/1 and Durham University. DiRAC is part of the National E-Infrastructure. Support was also received via the Interuniversity Attraction Poles Programme initiated by the Belgian Science Policy Office ([AP P7/08 CHARM]), the National Science Foundation under Grant No. NSF PHY11-25915, and the UK Science and Technology Facilities Council (grant numbers ST/F001166/1 and ST/I000976/1) via rolling and consolidating grants awarded to the ICC. We acknowledge the Virgo Consortium for making their simulation data available. The EAGLE simulations were performed using the DiRAC-2 facility at Durham, managed by the ICC, and the PRACE facility Curie based in France at TGCC, CEA, Bruyeres-le-Chatel. This research was supported in part by the National Science Foundation under Grant No. NSF PHY11-25915. Parts of this research were conducted by the Australian Research Council Centre of Excellence for All-sky Astrophysics (CAASTRO), through project number CE110001020, and supported by the Australian Research Council Discovery Project 160102235.

REFERENCES

- Bacon R., Accardo M., Adjali L., Anwand H., Bauer S., Biswas I., Blaizot J., Boudon e. a., 2010, in *Proc. SPIE*, Vol. 7735, Ground-based and Airborne Instrumentation for Astronomy III, p. 773508
- Bahé Y. M., Crain R. A., Kauffmann G., Bower R. G., Schaye J., Furlong M., Lagos C., Schaller M. et al, 2016, *MNRAS*, 456, 1115
- Barnes J., Efstathiou G., 1987, *ApJ*, 319, 575
- Barnes J. E., 1988, *ApJ*, 331, 699
- Baugh C. M., 2006, *Reports on Progress in Physics*, 69, 3101
- Bekki K., 1998, *ApJ*, 502, L133
- Bluck A. F. L., Conselice C. J., Bouwens R. J., Daddi E., Dickinson M., Papovich C., Yan H., 2009, *MNRAS*, 394, L51
- Bluck A. F. L., Conselice C. J., Buitrago F., Grützbauch R., Hoyos C., Mortlock A., Bauer A. E., 2012, *ApJ*, 747, 34
- Bois M., Emsellem E., Bournaud F., Alatalo K., Blitz L., Bureau M., Cappellari M., Davies R. L. et al, 2011, *MNRAS*, 416, 1654
- Bower R. G., Benson A. J., Malbon R., Helly J. C., Frenk C. S., Baugh C. M., Cole S., Lacey C. G., 2006, *MNRAS*, 370, 645
- Boylan-Kolchin M., Ma C.-P., Quataert E., 2005, *MNRAS*, 362, 184
- Bundy K., Bershady M. A., Law D. R., Yan R., Drory N., Macdonald N., Wake D. A., Cherinka B. et al, 2015, *ApJ*, 798, 7
- Bundy K., Fukugita M., Ellis R. S., Targett T. A., Belli S., Kodama T., 2009, *ApJ*, 697, 1369
- Burkert A., Förster Schreiber N. M., Genzel R., Lang P., Tacconi L. J., Wisnioski E., Wuyts S., Bandara K. et al, 2016, *ApJ*, 826, 214
- Cappellari M., Emsellem E., Krajnović D., McDermid R. M., Scott N., Verdoes Kleijn G. A., Young L. M., Alatalo K. et al, 2011, *MNRAS*, 413, 813
- Catelan P., Theuns T., 1996, *MNRAS*, 282, 436
- Coccato L., Gerhard O., Arnaboldi M., Das P., Douglas N. G., Kuijken K., Merrifield M. R., Napolitano N. R. et al, 2009, *MNRAS*, 394, 1249
- Cole S., Lacey C. G., Baugh C. M., Frenk C. S., 2000, *MNRAS*, 319, 168
- Cortese L., Fogarty L. M. R., Bekki K., van de Sande J., Couch W., Catinella B., Colless M., Obreschkow D. et al, 2016, *ArXiv:1608.00291*
- Cox T. J., Dutta S. N., Di Matteo T., Hernquist L., Hopkins P. F., Robertson B., Springel V., 2006, *ApJ*, 650, 791
- Crain R. A., Bahe Y. M., Lagos C. d. P., Rahmati A., Schaye J., McCarthy I. G., Marasco A., Bower R. G. et al, 2016, *ArXiv:1604.06803*
- Crain R. A., Schaye J., Bower R. G., Furlong M., Schaller M., Theuns T., Dalla Vecchia C., Frenk C. S. et al, 2015, *MNRAS*, 450, 1937
- Croom S. M., Lawrence J. S., Bland-Hawthorn J., Bryant J. J., Fogarty L., Richards S., Goodwin M., Farrell T. et al, 2012, *MNRAS*, 421, 872
- Danovich M., Dekel A., Hahn O., Ceverino D., Primack J., 2015, *MNRAS*, 449, 2087
- Davis T. A., Rowlands K., Allison J. R., Shabala S. S., Ting Y.-S., Lagos C. d. P., Kaviraj S., Bourne N. et al, 2015, *MNRAS*, 449, 3503
- De Lucia G., Springel V., White S. D. M., Croton D., Kauffmann G., 2006, *MNRAS*, 366, 499
- Di Matteo P., Jog C. J., Lehnert M. D., Combes F., Semelin B., 2009, *A&A*, 501, L9
- Dolag K., Borgani S., Murante G., Springel V., 2009, *MNRAS*, 399, 497
- Dubois Y., Peirani S., Pichon C., Devriendt J., Gavazzi R., Welker C., Volonteri M., 2016, *MNRAS*, 463, 3948
- Emsellem E., Cappellari M., Krajnović D., Alatalo K., Blitz L., Bois M., Bournaud F., Bureau M. et al, 2011, *MNRAS*, 414, 888
- Emsellem E., Cappellari M., Krajnović D., van de Ven G., Bacon R., Bureau M., Davies R. L., de Zeeuw P. T. et al, 2007, *MNRAS*, 379, 401
- Fall S. M., 1983, in *IAU Symposium*, Vol. 100, Internal Kinematics and Dynamics of Galaxies, Athanassoula E., ed., pp. 391–398
- Farouki R. T., Shapiro S. L., 1982, *ApJ*, 259, 103
- Foster C., Spitler L. R., Romanowsky A. J., Forbes D. A., Pota V., Bekki K., Strader J., Proctor R. N. et al, 2011, *MNRAS*, 415, 3393
- Furlong M., Bower R. G., Crain R. A., Schaye J., Theuns T., Trayford J. W., Qu Y., Schaller M. et al, 2015a, *ArXiv:1510.05645*
- Furlong M., Bower R. G., Theuns T., Schaye J., Crain R. A., Schaller M., Dalla Vecchia C., Frenk C. S. et al, 2015b, *MNRAS*, 450, 4486
- Genel S., Fall S. M., Hernquist L., Vogelsberger M., Snyder G. F., Rodriguez-Gomez V., Sijacki D., Springel V., 2015, *ApJ*, 804, L40
- Haardt F., Madau P., 2001, in *Clusters of Galaxies and the High Redshift Universe Observed in X-rays*, Neumann D. M., Tran J. T. V., eds., p. 64
- Hearin A. P., Behroozi P. S., van den Bosch F. C., 2016, *MNRAS*, 461, 2135
- Heyl J. S., Hernquist L., Spergel D. N., 1996, *ApJ*, 463, 69
- Jesseit R., Cappellari M., Naab T., Emsellem E., Burkert A., 2009, *MNRAS*, 397, 1202
- Jiang L., Helly J. C., Cole S., Frenk C. S., 2014, *MNRAS*, 440, 2115
- Johansson P. H., Naab T., Burkert A., 2009, *ApJ*, 690, 802

- Kauffmann G., Li C., Zhang W., Weinmann S., 2013, *MNRAS*, 430, 1447
- Lagos C. D. P., Cora S. A., Padilla N. D., 2008, *MNRAS*, 388, 587
- Lagos C. d. P., Crain R. A., Schaye J., Furlong M., Frenk C. S., Bower R. G., Schaller M., Theuns T. et al, 2015, *MNRAS*, 452, 3815
- Lagos C. d. P., Theuns T., Schaye J., Furlong M., Bower R. G., Schaller M., Crain R. A., Trayford J. W. et al, 2016, *MNRAS*, 459, 2632
- Lagos C. d. P., Theuns T., Stevens A. R. H., Cortese L., Padilla N. D., Davis T. A., Contreras S., Croton D., 2017, *MNRAS*, 464, 3850
- López-Sanjuan C., Le Fèvre O., Ilbert O., Tasca L. A. M., Bridge C., Cucciati O., Kampczyk P., Pozzetti L. et al, 2012, *A&A*, 548, A7
- Lotz J. M., Jonsson P., Cox T. J., Primack J. R., 2010, *MNRAS*, 404, 590
- Makino J., Hut P., 1997, *ApJ*, 481, 83
- McAlpine S., Helly J. C., Schaller M., Trayford J. W., Qu Y., Furlong M., Bower R. G., Crain R. A. et al, 2015, *ArXiv:1510.01320*
- McNeil E. K., Arnaboldi M., Freeman K. C., Gerhard O. E., Coccatto L., Das P., 2010, *A&A*, 518, A44
- Mo H. J., Mao S., White S. D. M., 1998, *MNRAS*, 295, 319
- Moreno J., Torrey P., Ellison S. L., Patton D. R., Bluck A. F. L., Bansal G., Hernquist L., 2015, *MNRAS*, 448, 1107
- Naab T., Jesseit R., Burkert A., 2006a, *MNRAS*, 372, 839
- Naab T., Khochfar S., Burkert A., 2006b, *ApJ*, 636, L81
- Naab T., Oser L., Emsellem E., Cappellari M., Krajnović D., McDermid R. M., Alatalo K., Bayet E. et al, 2014, *MNRAS*, 444, 3357
- Navarro J. F., Frenk C. S., White S. D. M., 1997, *ApJ*, 490, 493
- Navarro J. F., White S. D. M., 1994, *MNRAS*, 267, 401
- Obreschkow D., Glazebrook K., 2014, *ApJ*, 784, 26
- Pawlik A. H., Schaye J., 2008, *MNRAS*, 389, 651
- Pedrosa S. E., Tissera P. B., 2015, *A&A*, 584, A43
- Peirani S., Crockett R. M., Geen S., Khochfar S., Kaviraj S., Silk J., 2010, *MNRAS*, 405, 2327
- Planck Collaboration, 2014, *A&A*, 571, A16
- Qu Y., Helly J. C., Bower R. G., Theuns T., Crain R. A., Frenk C. S., Furlong M., McAlpine S. et al, 2017, *MNRAS*, 464, 1659
- Rahmati A., Pawlik A. H., Raicevic M., Schaye J., 2013, *MNRAS*, 430, 2427
- Robertson B., Bullock J. S., Cox T. J., Di Matteo T., Hernquist L., Springel V., Yoshida N., 2006, *ApJ*, 645, 986
- Robotham A. S. G., Driver S. P., Davies L. J. M., Hopkins A. M., Baldry I. K., Agius N. K., Bauer A. E., Bland-Hawthorn J. et al, 2014, *MNRAS*, 444, 3986
- Rodriguez-Gomez V., Sales L. V., Genel S., Pillepich A., Zjupa J., Nelson D., Griffen B., Torrey P. et al, 2016, *ArXiv:1609.09498*
- Romanowsky A. J., Fall S. M., 2012, *ApJS*, 203, 17
- Romanowsky A. J., Strader J., Spitler L. R., Johnson R., Brodie J. P., Forbes D. A., Ponman T., 2009, *AJ*, 137, 4956
- Schaller M., Dalla Vecchia C., Schaye J., Bower R. G., Theuns T., Crain R. A., Furlong M., McCarthy I. G., 2015, *MNRAS*, 454, 2277
- Schaye J., Crain R. A., Bower R. G., Furlong M., Schaller M., Theuns T., Dalla Vecchia C., Frenk C. S. et al, 2015, *MNRAS*, 446, 521
- Serra P., Oosterloo T., Morganti R., Alatalo K., Blitz L., Bois M., Bournaud F., Bureau M. et al, 2012, *MNRAS*, 2823
- Sokolowska A., Capelo P. R., Fall S. M., Mayer L., Shen S., Bonoli S., 2016, *ArXiv:1612.07362*
- Sparre M., Springel V., 2016a, *ArXiv:1610.03850*
- , 2016b, *MNRAS*, 462, 2418
- Springel V., 2000, *MNRAS*, 312, 859
- , 2005, *MNRAS*, 364, 1105
- Springel V., Wang J., Vogelsberger M., Ludlow A., Jenkins A., Helmi A., Navarro J. F., Frenk C. S. et al, 2008, *MNRAS*, 391, 1685
- Springel V., White S. D. M., Tormen G., Kauffmann G., 2001, *MNRAS*, 328, 726
- Stevens A. R. H., Croton D. J., Mutch S. J., 2016a, *MNRAS*, 461, 859
- Stevens A. R. H., Lagos C. d. P., Contreras S., Croton D. J., Padilla N. D., Schaller M., Schaye J., Theuns T., 2016b, *ArXiv:1608.04389*
- Taranu D. S., Dubinski J., Yee H. K. C., 2013, *ApJ*, 778, 61
- Teklu A. F., Remus R.-S., Dolag K., Beck A. M., Burkert A., Schmidt A. S., Schulze F., Steinborn L. K., 2015, *ApJ*, 812, 29
- Toomre A., 1977, in *Evolution of Galaxies and Stellar Populations*, Tinsley B. M., Larson D. Campbell R. B. G., eds., p. 401
- Toomre A., Toomre J., 1972, *ApJ*, 178, 623
- Trayford J. W., Theuns T., Bower R. G., Schaye J., Furlong M., Schaller M., Frenk C. S., Crain R. A. et al, 2015, *MNRAS*, 452, 2879
- Veale M., Ma C.-P., Thomas J., Greene J. E., McConnell N. J., Walsh J., Ito J., Blakeslee J. P. et al, 2017, *MNRAS*, 464, 356
- Vogelsberger M., Genel S., Springel V., Torrey P., Sijacki D., Xu D., Snyder G., Nelson D. et al, 2014, *MNRAS*, 444, 1518
- Wang J., Serra P., Józsa G. I. G., Koribalski B., van der Hulst T., Kamphuis P., Li C., Fu J. et al, 2015, *MNRAS*, 453, 2399
- Welker C., Dubois Y., Pichon C., Devriendt J., Chisari E. N., 2015, *ArXiv:1512.00400*
- White S. D. M., 1978, *MNRAS*, 184, 185
- White S. D. M., Rees M. J., 1978, *MNRAS*, 183, 341
- Young L. M., Bureau M., Davis T. A., Combes F., McDermid R. M., Alatalo K., Blitz L., Bois M. et al, 2011, *MNRAS*, 414, 940
- Zavala J., Frenk C. S., Bower R., Schaye J., Theuns T., Crain R. A., Trayford J. W., Schaller M. et al, 2016, *MNRAS*, 460, 4466
- Zavala J., Okamoto T., Frenk C. S., 2008, *MNRAS*, 387, 364

APPENDIX A: RADIAL J_{STARS} PROFILES AT FINE TIME INTERVALS BETWEEN OUTPUTS

The standard trees of EAGLE connect 29 epochs for which snapshots are saved (including all particle properties). The time span between snapshots can range from ≈ 0.3 Gyr to ≈ 1 Gyr. Galaxy mergers, however, may require finer time intervals between snapshots to follow in more detail how the merger evolves. Schaye et al. (2015) showed that in addition to the snapshots described above, the EAGLE simulations also record 400 *snipshots*, in the redshift range $0 \leq z \leq 20$, saving fewer gas particle properties. In our case, we would like to measure the mean radial j_{stars} profile in galaxies during and after the merger, and the information stored in snipshots allows us to do this. Owing to the computational expense of applying SUBFIND to the outputs of EAGLE only 200 even-numbered snipshots of the simulation suite were catalogued. This decreases the time span between snipshots to ≈ 0.05 Gyr to 0.3 Gyr.

Here, we take all the snipshots between $z \approx 0.5$ and $z \approx 1$

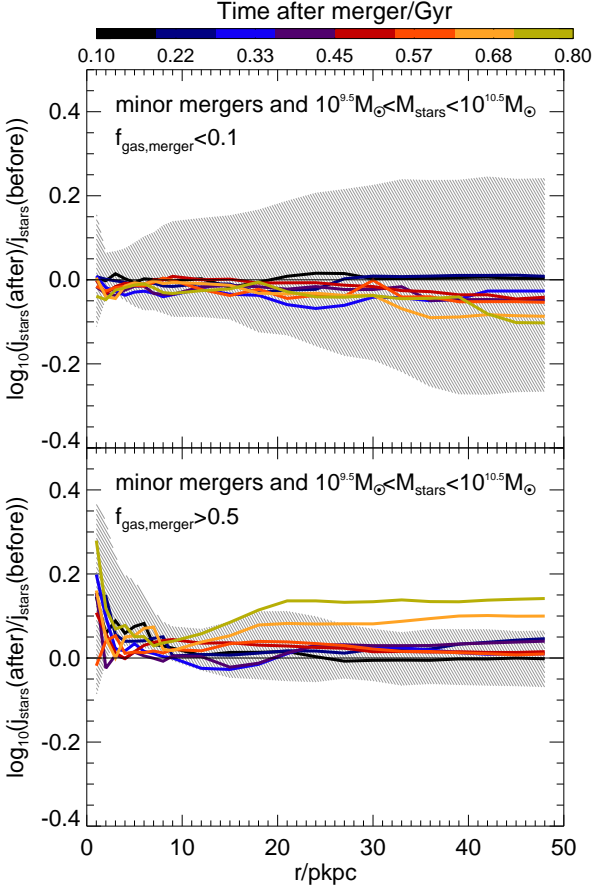


Figure A1. The ratio between the mean j_{stars} after and before galaxy mergers, measured in an aperture r , as a function of r . We measure j_{stars} after the merger in 8 subsequent snapshots after the merger. Each snapshot samples a timestep of ≈ 0.1 Gyr. Here we show galaxies with $10^{9.5} M_{\odot} < M_{\text{stars}} < 10^{10.5} M_{\odot}$ that went through a minor merger in the redshift range $0.65 \lesssim z \lesssim 0.75$. The top panel shows the subsample of gas-poor mergers, while the bottom panel shows gas-rich mergers. Lines show the median, with the colour indicating the time after the merger, as shown in the colorbar at the top. For simplicity we only show the 25th-75th percentile range (shaded region) for the first snapshot after the merger. For reference, the horizontal lines show no change on $j_{\text{stars}}(r)$, and so values above the line show an increase in j_{stars} , while the opposite holds if below the line.

and select all galaxy mergers that took place in that redshift range. We focus on this range because it is roughly when gas-rich and gas-poor mergers happen in similar numbers (see Fig. 2) in the Ref-L0100N1504 simulation. We calculate the radial j_{stars} profiles before and after the galaxy mergers (from ≈ 0.1 to ≈ 0.8 Gyr after a minor merger, in timesteps of ≈ 0.1 Gyr). We show in Fig A1 the radial j_{stars} profiles after the merger divided by the profiles before the merger for galaxies with $10^{9.5} M_{\odot} < M_{\text{stars}} < 10^{10.5} M_{\odot}$. We separate mergers into gas-rich and gas-poor. Our idea here is to test if the results of Fig. 11 are affected by how fine the time interval between outputs is in the simulation. We find that gas-poor minor mergers systematically decrease j_{stars} over the entire radial range, while gas-rich minor mergers help increase j_{stars} in the central parts of galaxies, while changing only mildly j_{stars} at $r \gtrsim 10$ pkpc. Note that at later times ($\gtrsim 0.6$ Gyr after the merger) j_{stars} in the outer regions starts increasing faster. We interpret this

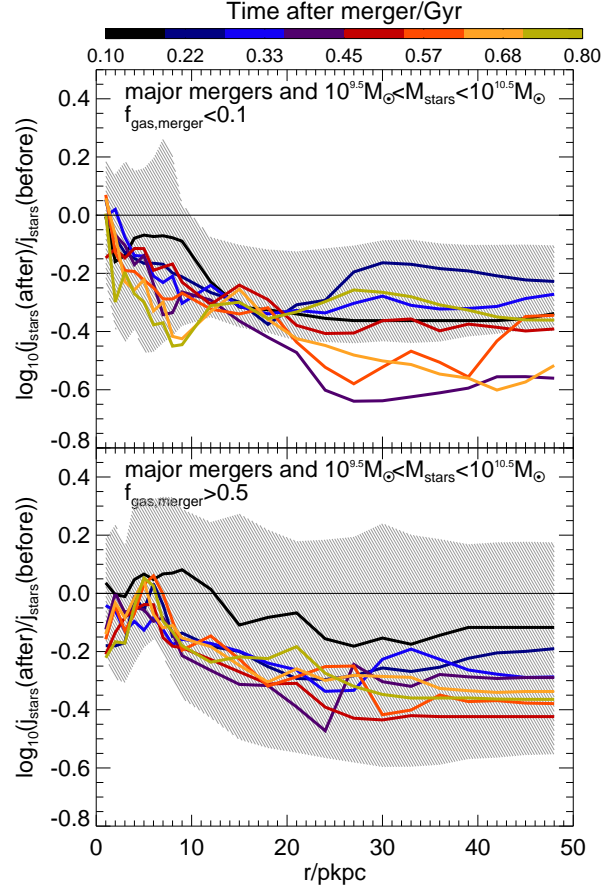


Figure A2. As Fig. A1 but for major mergers.

behaviour as resulting from continuing star formation, rather than due to the galaxy merger.

Fig. A2 is as Fig. A1 but for major mergers. Although the trends are noisy, there is a systematic effect of gas-poor major mergers to decrease j_{stars} over the entire radial range probed here. Gas-rich major mergers tend to preferentially reduce j_{stars} at $r \gtrsim 10$ kpc, while not affecting the inner regions of galaxies much. Although noisy, one could even argue that j_{stars} increases in the inner regions of galaxies as a result of a gas-rich major merger. We find that the results here are broadly consistent with those presented in the top panels of Fig. 11, and thus we conclude that finer time resolution only confirms the behaviour we analysed there.

APPENDIX B: THE EFFECT OF REDSHIFT, STELLAR MASS AND APERTURE IN J_{STARS}

In § 3.2, we stacked all of the galaxy mergers that take place in galaxies with $M_{\text{stars}} \geq 10^{9.5} M_{\odot}$ and in the redshift range $0 \leq z \leq 2.5$. This may introduce significant biases due to the time-stepping of the simulation (different snapshots cover different timescales), and also due to galaxies having very different sizes at different cosmic epochs. In order to quantify that bias, we analyse galaxy mergers at different cosmic epochs and stellar mass bins, separated into minor and major and into wet and dry mergers in Fig. B1. We first compare the distributions as a function of gas-richness, and we find that there is no statistical difference between

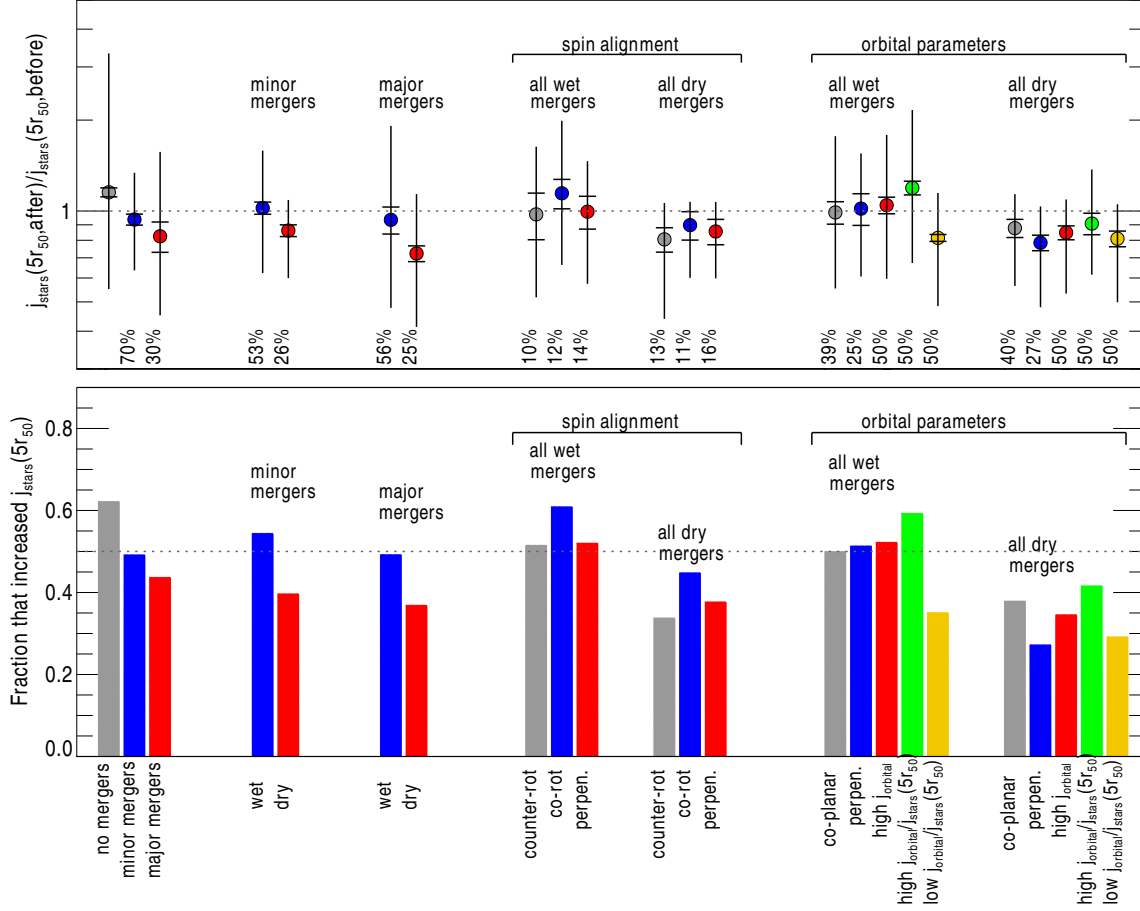


Figure B2. As Fig. 10 but for $j_{\text{stars}}(5r_{50})$.

the wet and dry minor merger populations at different redshifts. The Kolmogorov-Smirnov p -values are in the range $\approx 0.2 - 0.9$ when we compare wet or dry merger populations at different redshifts. When we compare wet vs. dry minor mergers at different redshift, we find that the differences seen in Fig. 10 are always present with high statistical significance (p -values are $\lesssim 10^{-4}$). When we analyse different stellar mass bins we reach the same conclusion. Thus, we can comfortably assume that stacking minor mergers at different redshift does not introduce any significant bias to our analysis. In the case of major mergers, we see more variations between the subsamples at different redshifts and stellar masses, but the difference between dry and wet mergers is still the most important one statistically (with p -values $\lesssim 10^{-3}$).

Fig. B2 shows the ratio between $j_{\text{stars}}(5r_{50})$ after and before mergers (top panel) and the frequency in which mergers increase $j_{\text{stars}}(5r_{50})$ (bottom panel). We find that the results shown here are similar to those of Fig. 10 for j_{stars} measured within r_{50} .

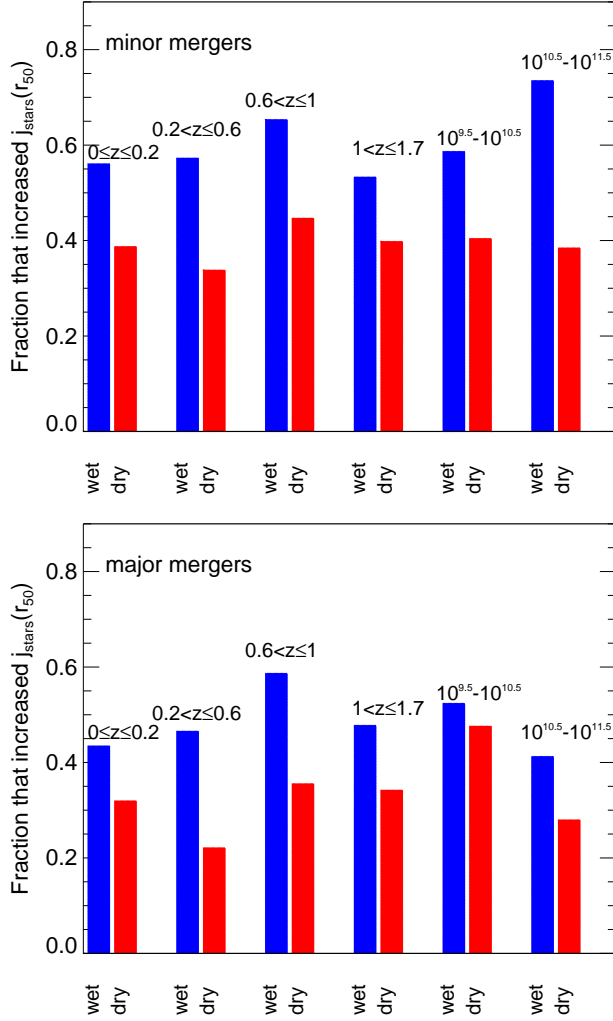


Figure B1. *Top panel:* Fraction of galaxies that display an increase in their $j_{\text{stars}}(r_{50})$ during minor mergers at different redshifts and in two bins of stellar mass, split into wet and dry mergers, as labelled. *Bottom panel:* As in the top panel but for major mergers.